cmgh
CELLULAR AND MOLECULAR GASTROENTEROLOGY AND HEPATOLOGY

ORIGINAL RESEARCH

Intraepithelial Lymphocytes Suppress Intestinal Tumor Growth by Cell-to-Cell Contact via CD103/E-Cadherin Signal

Ryo Morikawa,[1] Yasuhiro Nemoto,[1,2] Yuki Yonemoto,[1] Shohei Tanaka,[1] Yuria Takei,[1] Shigeru Oshima,[1] Takashi Nagaishi,[2] Kiichiro Tsuchiya,[1] Kengo Nozaki,[1] Tomohiro Mizutani,[1] Tetsuya Nakamura,[3] Mamoru Watanabe,[1,4] and Ryuichi Okamoto[1]

[1]Department of Gastroenterology and Hepatology, Graduate School, [2]Department of Advanced Therapeutics for GI Diseases, [4]Advanced Research Institute, Tokyo Medical and Dental University, Tokyo, Japan; [3]Department of Organoid Research and Development, Juntendo University, Tokyo, Japan

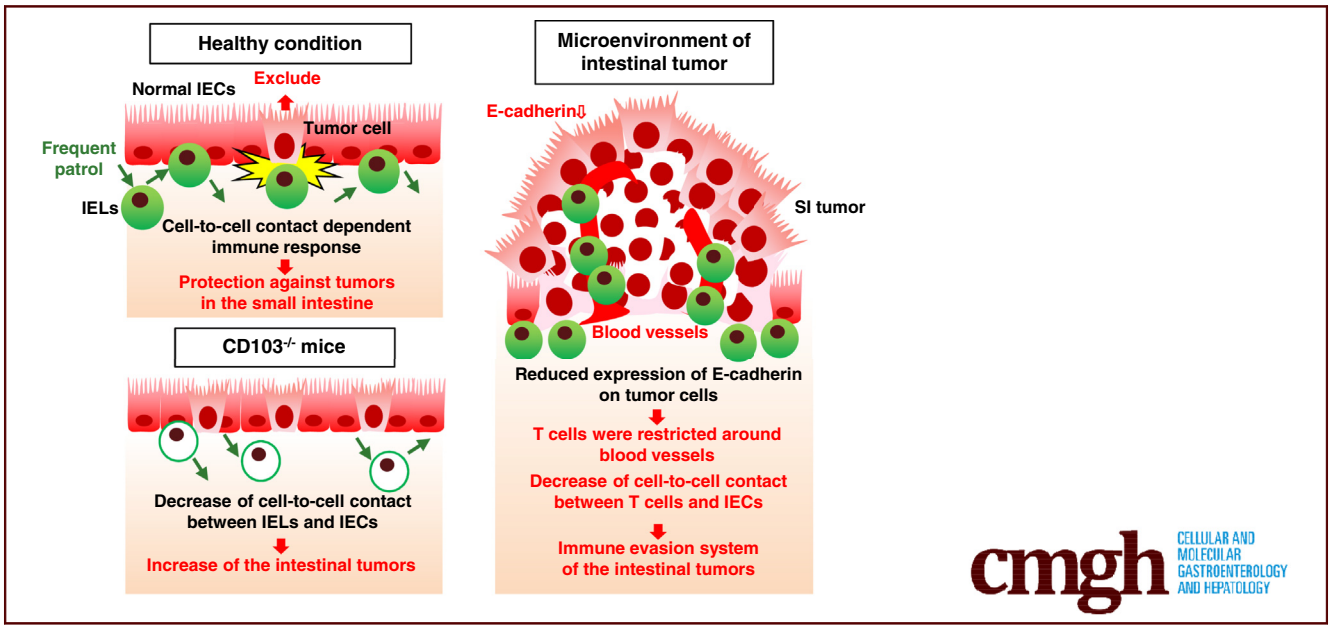

SUMMARY

By developing the novel in vivo live imaging system and in vitro co-culture system, we proved that intraepithelial lymphocytes suppress intestinal tumor growth by cell-to-cell contact via CD103/E-cadherin signal.

BACKGROUND & AIMS: The reason why small intestinal cancer is rarer than colorectal cancer is not clear. We hypothesized that intraepithelial lymphocytes (IELs), which are enriched in the small intestine, are the closest immune cells to epithelial cells, exclude tumor cells via cell-to-cell contact.

METHODS: We developed DPE-green fluorescent protein (DPE-GFP) × adenomatous polyposis coli; multiple intestinal neoplasia (APC^{min}) mice, which is a T-cell–reporter mouse with spontaneous intestinal tumors. We visualized the dynamics of IELs in the intestinal tumor microenvironment and the interaction between IELs and epithelial cells, and the roles of cell-to-cell contact in anti-intestinal tumor immunity using a novel in vivo live-imaging system and a novel in vitro co-culture system.

RESULTS: In the small intestinal tumor microenvironment, T-cell movement was restricted around blood vessels and the frequency of interaction between IELs and epithelial cells was reduced. Genetic deletion of CD103 decreased the frequency of interaction between IELs and epithelial cells, and increased the number of small intestinal tumors. In the co-culture system, wild-type IELs expanded and infiltrated to intestinal tumor organoids from APC^{min} mice and reduced the viability of them, which was cell-to-cell contact and CD103 dependent.

CONCLUSIONS: The abundance of IELs in the small intestine may contribute to a low number of tumors, although this system may not work in the colon because of the sparseness of IELs. Strategies to increase the number of IELs in the colon or enhance cell-to-cell contact between IELs and epithelial cells may be effective for the prevention of intestinal tumors in patients with a high cancer risk. *(Cell Mol Gastroenterol Hepatol 2021;11:1483–1503; https://doi.org/10.1016/j.jcmgh.2021.01.014)*

Keywords: IELs; In Vivo Live Imaging; Organoid.

Since the development of immune checkpoint inhibitors for cancer treatment, such as anti–programmed death receptor-1- antibodies and anti-cytotoxic T-lymphocyte antigen-4 antibodies, immunotherapy has been the focus of attention as a next-generation cancer treatment.[1,2] The remarkable effectiveness of these drugs suggests that the immune system has the potential to exclude cancer by itself. However, the tumor microenvironment has various immune evasion systems.[3,4] Therefore, clarification of these immune evasion systems is key for the development of more effective cancer immunotherapy.

Colorectal cancer is one of the most common cancers in many countries.[5,6] The mortality rate of colorectal cancer is high and the number of cases is still increasing. The incidence rate of small intestinal cancer is approximately 3% that of colorectal cancer.[7] The reason underlying the low incidence rate of small intestinal cancer has not been clarified.

Gut microbes are the first candidate as a possible reason underlying the difference in intestinal cancer rates because the colon has at least 10^4-fold higher levels of gut microbes compared with the small intestine.[8] Research has shown a strong relationship between gut microbes and intestinal tumors.[9–11] One study showed that low-grade inflammation of the intestine induced by dysbiosis promotes tumorigenesis.[9] In contrast, even in the germ-free condition, adenomatous polyposis coli; multiple intestinal neoplasia(APC^{min}) mice, which have a mutation in *APC* and develop spontaneous tumors in both the small and large intestine,[10] develop 60% as many small intestinal tumors as in the specific pathogen-free condition.[11] These findings suggest that the small intestine contains other factors that suppress tumorigenesis.

Although the mechanism by which intestinal tumors develop has not been completely clarified yet, the first step of the process involves single-cell level of tumorigenesis caused by carcinogenic factors, such as chemical substances or inflammation. In healthy conditions, immune cells actively eliminate these aberrant cells, and cytotoxic T cells play important roles in this antitumor immunity.[12] Studies have shown a considerable number of $CD3^+$ T cells in the microenvironment of intestinal tumors.[13] In addition, the effectiveness of immune checkpoint inhibitors, which enhance the antitumor activity of T cells, proved the importance of T cells in antitumor immunity.

The intestine has a large number of unique T cells, called intraepithelial lymphocytes (IELs). IELs are the closest immune cells to intestinal epithelial cells (IECs), and these cells exist within the intestinal epithelial monolayer.[14] IELs include not only conventional $CD4^+$ or $CD8^+$ T cells, also called *induced IELs*, but also unconventional $\gamma\delta$ T cells or $CD4^-CD8\alpha\beta^-TCR\alpha\beta^+$ T cells (double-negative T; DN T), also called *natural IELs*.[14] Natural IELs have self-reactive T-cell receptors (TCRs), granzyme A and B, and high cytotoxic activity. However, their physiological roles in the intestinal immune system still are enigmatic. Although previously thought to be fixed, $\gamma\delta$-IELs dynamically move and attach to many epithelial cells. Notably, the small intestine has 10-fold higher levels of IELs compared with the colon.[15] Therefore, we hypothesized that IELs, which are abundant in the small intestine and the closest immune cells to epithelial cells, may be in frequent contact with epithelial cells, patrol epithelial cells, and exclude single-cell–level tumor cells via cell-to-cell contact to inhibit tumor growth in the small intestine.

Although IELs are thought to play important roles for protective immunity and quality management and regeneration of IECs via cytokines,[14] their roles in antitumor immunity have not been fully studied. In experiments using $RAG^{-/-}$, $TCR\beta^{-/-}$, or $TCR\delta^{-/-}$ mice,[16,17] the effects of systemic deletion of T cells on the number of intestinal tumors were examined; however, the effect of IEL-specific deletion has not been examined. Although static analyses showed that T cells exist within the intestinal tumor microenvironment, their dynamics within the tumor microenvironment have not been explored.

Here, we visualized the dynamics of T cells in the intestinal tumor microenvironment and the interaction between IELs and epithelial cells and investigated the role of cell-to-cell contact between IELs and epithelial cells in anti-intestinal tumor immunity using a novel in vivo live-imaging system of IELs and intestinal tumor and novel in vitro co-culture system of IELs and small intestinal tumor organoids.

Results

Visualization of the 3-Dimensional Distribution of T Cells in the Small Intestinal Tumor Microenvironment by Tissue Clearing

As an intestinal tumor model, we chose the APC^{min} mouse, which develops a large number of intestinal tumors because of a mutation in the *APC* gene. The APC^{min} mouse is one of the most common spontaneous intestinal tumor models and the model that develops both small intestinal tumors and colon tumors. As a T-cell–reporter mouse, we selected the DPE-green fluorescent protein (DPE-GFP) mouse, in which $CD3^+$ T cells express GFP.[18] We crossed APC^{min} and DPE–GFP mice to generate DPE–GFP $\times$ APC^{min} mice, which are T-cell–reporter mice with spontaneous intestinal tumors.

Abbreviations used in this paper: **APC^{min}, adenomatous polyposis coli multiple intestinal neoplasia; DN, double negative; DPE–GFP, DPE-green fluorescent protein; EGFP, enhanced green fluorescent protein; EMT, epithelial-mesenchymal transition; FITC, fluorescein isothiocyanate; HBSS, Hank's balanced salt solution; IEC, intestinal epithelial cell; IEL, intraepithelial lymphocyte; IHC, immunohistochemistry; IL, interleukin; Itgae, integrin alphaE; LPL, lamina propria lymphocytes; PBS, phosphate-buffered saline; 7-AAD, 7-Amino-Actinomycin D; TCR, T-cell receptor; TGF, transforming growth factor; 3D, 3-dimensional; WT, wild type.**

Most current article

© 2021 The Authors. Published by Elsevier Inc. on behalf of the AGA Institute. This is an open access article under the CC BY-NC-ND license (http://creativecommons.org/licenses/by-nc-nd/4.0/).
2352-345X
https://doi.org/10.1016/j.jcmgh.2021.01.014

Various kinds of immune cells infiltrate in the tumor microenvironment. Although many studies showed the 2-dimensional distribution of T cells in the microenvironment of intestinal tumors by immunohistochemistry (IHC), the 3-dimensional (3D) distribution of T cells has not been determined. Therefore, to visualize the 3D distribution of T cells in the microenvironment of small intestinal tumors, we performed tissue clearing in whole-mount tissues of small intestinal tumors (Figure 1*A*). After intravenous injection of DPE–GFP × APC^{min} mice with dextran-tetramethylrhodamine for vascular staining and Hoechst 33342 for nuclear staining, mice were killed. The small intestine was collected and processed as described in the Materials and Methods section, followed by analysis with a 2-photon microscope. By wide area imaging of tumor tissues, we could identify the tumor region as the area where villi coalesce and the ductal structure was not clear (Figure 1*B*). This area was not observed in tissues from control DPE–GFP mice (Figure 1*C*).

We next performed z-stack analysis of tumor tissues (Figure 1*D*–*I*, Supplementary Movies 1 and 2). Fewer T cells infiltrated in the small intestinal tumor microenvironment than in the normal mucosa (Figure 1*J*). Notably, the percentage of T cells merged to blood vessels was higher in the tumor tissues than in normal tissues, which suggests that localization of T cells in the tumor microenvironment is restricted (Figure 1*K*).

Visualization of T-Cell Dynamics in the Intestinal Tumor Microenvironment by the In Vivo Live-Imaging System

Although our results showed the 3D distribution of T cells in the intestinal tumor microenvironment, we were unable to observe the movement of T cells, which is a limitation of fixed samples. Therefore, we next developed a novel in vivo live-imaging system to visualize T-cell dynamics for small intestinal tumors (Figure 2*A*). After intravenous injection of DPE–GFP × APC^{min} mice with Hoechst 33342 and dextran–Texas Red or dextran-tetramethylrhodamine, anesthetized mice were fixed on the customized stage with a warming plate. The small intestine was exposed, gently opened along the anti-mesenteric border, and analyzed with a 2-photon microscope. Similar to the tissue-clearing analyses, we could identify the tumor region as the area where villi coalesce, and the ductal structure was not clear by wide area imaging (Figure 2*B*), although these observations were not detected in tissues from control DPE–GFP mice (Figure 2*C*). We confirmed that this region meets the histologic definition of tumor by histologic analysis of samples fixed and stained with H&E after the in vivo live-imaging (Figure 2*D* and *E*). In the z-stack analysis, the ductal structure in the tumor was not clear (Figure 2*F* and *G*). We compared T-cell dynamics in the nontumor region of DPE–GFP × APC^{min} and control DPE–GFP mice (Figure 2*H* and *I*, Supplementary Movies 3 and 4). There were no differences in the speed, track length, confinement ratio, or total time of T cells in contact with epithelial cells between DPE–GFP × APC^{min} and control DPE–GFP mice (Figure 2*J*–*M*).

Movement of T Cells Is Restricted Around Blood Vessels and the Frequency of Interaction Between IELs and Epithelial Cells Is Reduced in the Small Intestinal Tumor Microenvironment

Next, we compared T-cell dynamics in the tumor and nontumor regions of DPE–GFP × APC^{min} mice (Figures 3*A*–*C* and Figure 4, Supplementary Movie 5). We confirmed the reduction of T cells in the tumor microenvironment. The number of T cells in contact with epithelial cells in the tumor region was smaller than those in the nontumor region (Figure 3*D*). Although there were no differences in the speed, track length, or confinement ratio between tumor and nontumor regions, the total time of T cells in contact with epithelial cells in the tumor region was less than that in the nontumor region (Figure 3*E*–*H*). Similar to the tissue-clearing analyses, movement of T cells in the tumor microenvironment was restricted around the blood vessels. Quantification confirmed this result (Figure 3*I*).

E-Cadherin Expression Is Reduced on the Tumor Epithelium of APC^{min} Mice Compared With Normal Epithelial Cells

Based on our observations that the frequency of interaction between IELs and epithelial cells in the tumor was reduced, we next considered whether the immune evasion system plays a role in this effect. Although the factor that regulates the interaction between IELs and epithelial cells is not fully clarified, the E-cadherin/CD103 signal is thought to play an important role.[19] IECs express E-cadherin, whereas most IELs express its ligand, CD103, also called *integrin* $\alpha E\beta 7$. Previous studies have shown that genetic deletion of CD103 reduced the number of IELs and the retention of $\gamma\delta$ T cells to IECs.[20,21] In contrast, expression of E-cadherin on some intestinal tumors is reduced as a result of epithelial–mesenchymal transition (EMT).[22,23] Therefore, we performed IHC to check the expression of E-cadherin on small intestinal tumors in APC^{min} mice. As shown in Figure 3*J* and *K*, the expression of E-cadherin on the tumor region was lower than that on normal epithelial cells. On the other hand, expression of CD103 on T cells was constitutive in the tumorous tissue or nontumorous tissue of APC^{min} mice (Figure 5*A*–*C*), which supports this hypothesis.

Frequency of Interaction Between IELs and Epithelial Cells Is Reduced in Mice With Genetic Deletion of CD103

Based on our earlier-described results, we hypothesized that the reduced frequency of the interaction between IELs and epithelial cells resulted from low expression of E-cadherin in APC^{min} mice. We thus next investigated changes in both the frequency of interaction between IELs and epithelial cells and intestinal tumor formation in integrin alphaE (Itgae)$^{-/-}$ mice, in which CD103, integrin $\alpha E\beta 7$, is deleted.

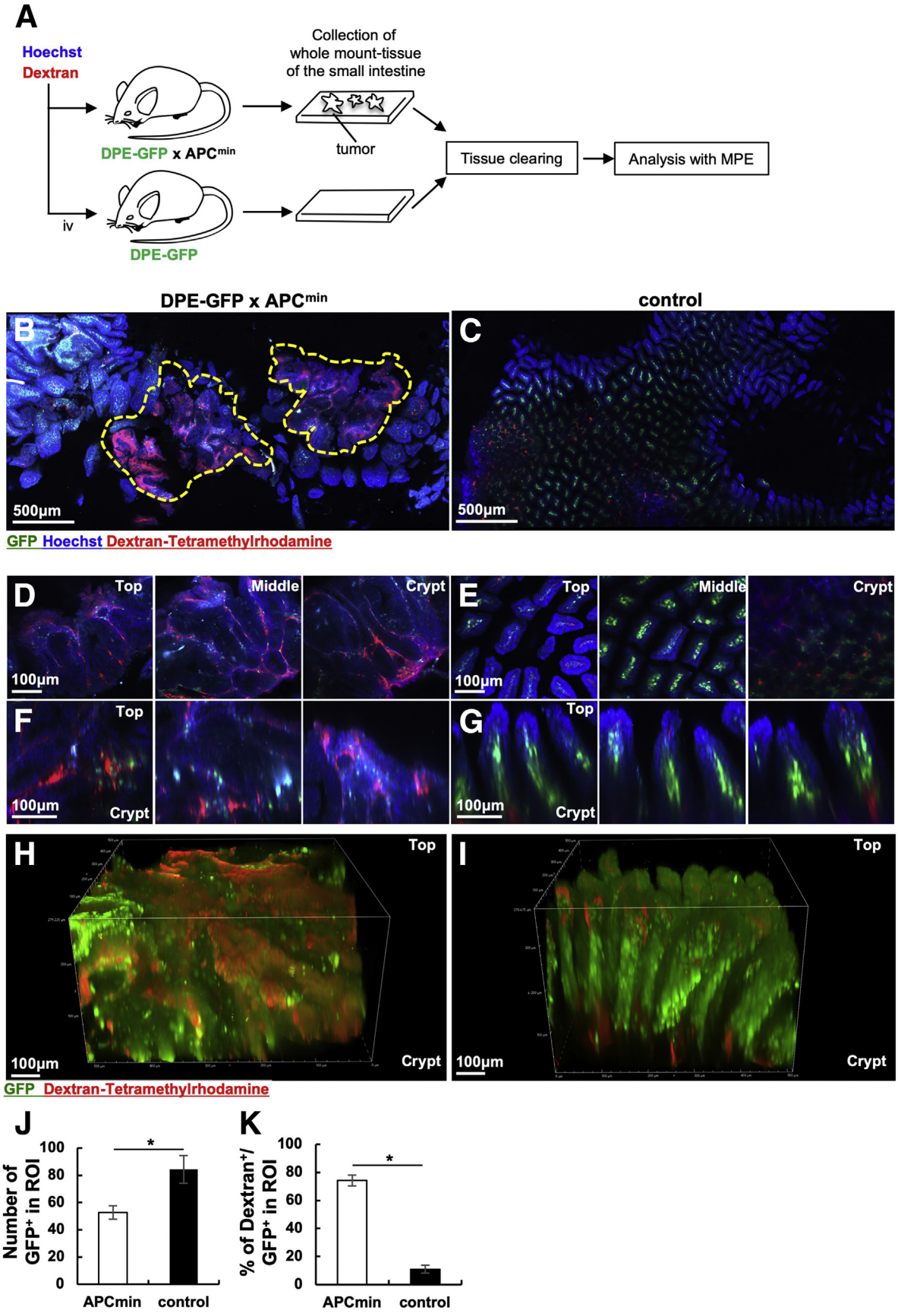
A
Hoechst
Dextran
Collection of
whole mount-tissue
of the small intestine
DPE-GFP x APCmin
tumor
Tissue clearing
Analysis with MPE
iv
DPE-GFP
DPE-GFP x APCmin
control
B
C
500μm
500μm
GFP Hoechst Dextran-Tetramethylrhodamine
D
E
F
G
H
I
Top
Middle
Crypt
100μm
GFP Dextran-Tetramethylrhodamine
J
K
Number of GFP+ in ROI
% of Dextran+/ GFP+ in ROI
100
80
60
40
20
0
*
APCmin
control

Although IHC showed that the number of IELs in the duodenum of Itgae$^{-/-}$ mice was reduced compared with controls,[20] the number of IELs in the entire small intestine and the number of each IEL fraction has not been investigated. We thus next performed flow cytometric analysis of the small intestine of Itgae$^{-/-}$ mice. Although the number of IELs in the small intestine of Itgae$^{-/-}$ mice was reduced compared with that of control littermate mice, consistent with the previous study, the reduction was approximately 25% at most (Figure 6*A*). The number of CD8^{+} and CD4^{+} T cells was reduced in Itgae$^{-/-}$ mice, whereas the numbers of $\gamma\delta$ and DN T cells did not change (Figure 6*A*). Among lamina propria lymphocytes (LPLs), the number of CD8^{+} T cells also was reduced, whereas the numbers of total T cells, $\gamma\delta$, DN, or CD4^{+} T cells did not change (Figure 6*B*). In addition, the number of regulatory T cells in the small intestine did not change in Itgae$^{-/-}$ mice (Figure 6*C*).

As mentioned earlier, it already has been proven that the retention of $\gamma\delta$ T cells to IECs was reduced in Itgae$^{-/-}$ mice with an in vivo live-imaging system. We next examined the interaction between IELs, which include not only $\gamma\delta$ but also other fractions, and epithelial cells of Itgae$^{-/-}$ mice by in vivo live-imaging (Figure 6*D–G*, Supplementary Movies 6 and 7). We crossed Itgae$^{-/-}$ mice and DPE–GFP mice and generated Itgae$^{-/-}$ × DPE–GFP mice. There was no difference in the speed, track length, or confinement ratio of T cells in contact with epithelial cells in the small intestine between Itgae$^{-/-}$ × DPE–GFP mice and control mice (Figure 6*H–J*). The total time of T cells in contact with epithelial cells in Itgae$^{-/-}$ × DPE–GFP mice was less than that in control mice (Figure 6*K*).

Mice With Genetic Deletion of CD103 Showed Increased Numbers of Small Intestinal Tumors

With this result, we decided to use Itgae$^{-/-}$ mice as a useful model to investigate the roles of IELs and the interaction between IELs and epithelial cells in intestinal tumorigenesis. We crossed Itgae$^{-/-}$ mice and APC^{min} mice to generate Itgae$^{-/-}$ × APC^{min} mice (Figure 7*A* and *B*). Although there was no difference in the mean tumor area, tumor number and total tumor area in the proximal, distal, and whole small intestine of Itgae$^{-/-}$ × APC^{min} mice were larger than those in control APC^{min} mice (Figure 7*C–E*).

Development of Co-culture System of IELs and Intestinal Tumor Organoids

Although our results showing increased numbers of small intestinal tumors in Itgae$^{-/-}$ × APC^{min} mice strongly supports our hypothesis that IELs play important roles in anti-intestinal tumor immunity, we cannot exclude the possibility that CD103 deletion in other immune cells might influence the tumor number. In addition, whether the reduction of numbers of IELs or the interaction between IELs and epithelial cells is more important for tumorigenesis is not clear. Therefore, to clarify the importance of the interaction between IELs and epithelial cells for anti-intestinal tumor immunity, we developed a novel co-culture system of both IELs and intestinal tumor organoids. Organoids are a recently developed useful tool for in vitro experiments with primary cells.[24] We previously reported a co-culture system of IELs and organoids derived from normal small intestine.[25] We modified this system and developed a novel co-culture system of IELs and intestinal tumor organoids derived from small intestinal tumors in APC^{min} mice (Figure 8*A*).

Antitumor Immune Response Is Provoked Between Co-cultured Wild-Type IELs and Intestinal Tumor Organoids

Organoids were derived from small intestinal tumors from APC^{min} mice or normal small intestine in control wild-type (WT) mice. IELs were sort-purified from the small intestine of enhanced green fluorescent protein (EGFP) mice. Organoids and IELs were co-cultured and analyzed on days 7–9 (Figure 8*B*). Time-lapse imaging showed that IELs moved toward and contacted both APC^{min} and WT organoids (Figures 8*C* and 9*A* and *B*, Supplementary Movies 8 and 9). Notably, the number of live epithelial cells recovered from APC^{min} organoids co-cultured with WT IELs was smaller than that of APC^{min} organoids alone, although there were no differences between WT organoids co-cultured with WT IELs and WT organoids alone (Figure 8*D*). In addition, IELs co-cultured with APC^{min} organoids expanded and the number increased compared with that of IELs co-cultured with WT organoids (Figure 8*E*).

To investigate the mechanism by which WT IELs reduced the viability of tumor organoids, we performed further experiments. First, we checked the expression of Ki67 in the epithelial cells derived from organoids in each group. As shown in Figure 10*A*, there was no difference in the percentages of Ki67^{+} in epithelial cells between APC^{min} organoids alone and the APC^{min} organoids and WT–IEL group. Next, we also checked the expression of Annexin V and 7-Amino-Actinomycin D (7-AAD) to detect the early apoptotic cells. However, there was no difference in the percentages of early apoptotic cells in epithelial cells between APC^{min} organoids alone and the APC^{min} organoid and WT-IEL group, either (Figure 10*B*).

Figure 1. (***See previous page***). **Visualization of 3D distribution of T cells in the microenvironment of small intestinal tumors shows T cells localized around blood vessels in the tumor.** (*A*) Experimental design. Wide area images of transparent small intestinal tissues of (*B*) DPE–GFP × APC^{min} or (*C*) DPE–GFP mice. Green, GFP; blue, Hoechst 33342; red, dextran-tetramethylrhodamine. Tomographic images of the x-axis and y-axis of small intestinal tissues of (*D*) DPE–GFP × APC^{min} or (*E*) DPE–GFP mice. Tomographic images of the x-axis and z-axis of small intestinal tissues of (*F*) DPE–GFP × APC^{min} or (*G*) DPE–GFP mice. 3D images of transparent small intestine of (*H*) DPE–GFP × APC^{min} or (*I*) DPE–GFP mice. (*J*) Number of T cells and (*K*) percentage of T cells in contact with blood vessel in the region of interest (ROI) (n = 3, each). Graphs show means ± SEM. *$P < .05$. MPE, multi-photon excitation microscopy.

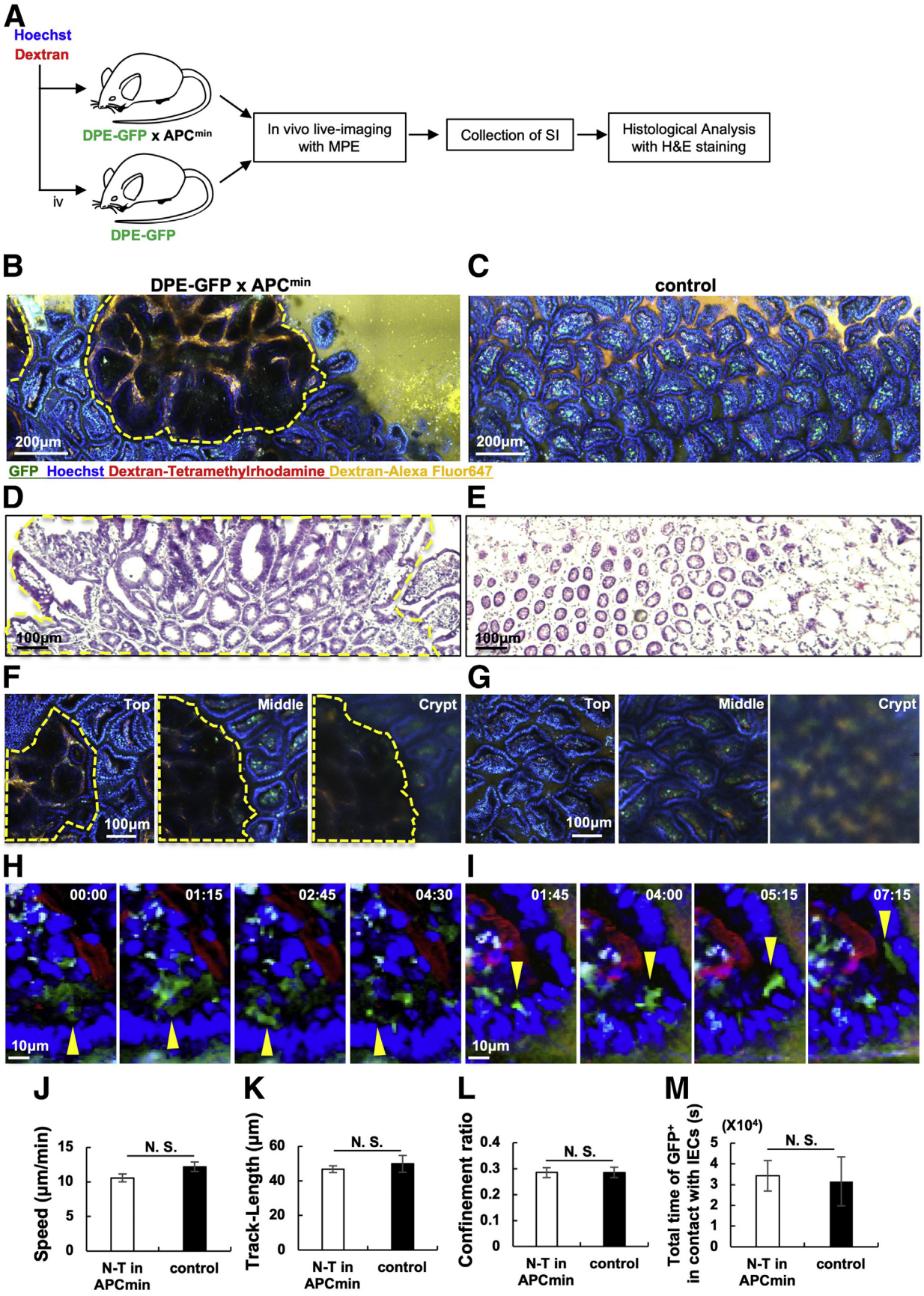
A
Hoechst
Dextran
DPE-GFP x APCmin
iv
DPE-GFP
In vivo live-imaging with MPE
Collection of SI
Histological Analysis with H&E staining
B
DPE-GFP x APCmin
200μm
C
control
200μm
GFP Hoechst Dextran-Tetramethylrhodamine Dextran-Alexa Fluor647
D
100μm
E
100μm
F
Top
Middle
Crypt
100μm
G
Top
Middle
Crypt
100μm
H
00:00
01:15
02:45
04:30
10μm
I
01:45
04:00
05:15
07:15
10μm
J
Speed (μm/min)
N. S.
N-T in APCmin
control
K
Track-Length (μm)
N. S.
N-T in APCmin
control
L
Confinement ratio
N. S.
N-T in APCmin
control
M
Total time of GFP+ in contact with IECs (s)
(X10⁴)
N. S.
N-T in APCmin
control

Next, we checked the amounts of cytokines produced in the supernatant of each group. Interestingly, a substantial amount of interferon-γ and tumor necrosis factor-α, but not of interleukin (IL)2, IL4, IL6, IL17A, IL10, or transforming growth factor (TGF)-β1 were detected in the supernatant of co-culture of WT-IELs and APC^{min} organoids (Figures 8*F* and *G* and 11).

Together, these findings suggest that the reduction of tumor cells in APC^{min} organoids and WT-IEL co-culture was the result of an antitumor immune response by WT IELs, rather than the suppression of proliferation, or the apoptosis of tumor cells caused by occupation of growth factors by expanded WT-IELs.

Surprisingly, different from the in vivo experiments (Figure 3*J* and *K*), the expression of E-cadherin on the APC^{min} organoids was not lower than that on WT organoids (Figure 12), which may lead to a stronger immune response in this co-culture system.

Finally, to investigate which subset of IELs is essential for the antitumor immune response, $\gamma\delta$, DN, CD4$^+$, and CD8$^+$ IELs were sort-purified and co-cultured with APC^{min} organoids. Although $\gamma\delta$ and CD8$^+$ IELs expanded more than DN or CD4$^+$ T cells (Figure 13*A*), there was no reduction in the number of live epithelial cells recovered from APC^{min} organoids co-cultured with each subset compared with those recovered from APC^{min} organoids cultured alone (Figure 13*B*), which suggests that cooperation of each fraction is essential for the effective antitumor immune response.

Antitumor Immune Response of IELs Against Intestinal Tumor Organoids Is Cell-to-Cell Contact–Dependent

As shown in Figure 8*F* and *G*, humoral factors, such as interferon-γ or tumor necrosis factor-α, seem to play important roles for the antitumor immune response in this co-culture system. Therefore, to determine the importance of cell-to-cell contact between IELs and IECs, we performed a separate culture experiment. Organoids derived from small intestinal tumors from APC^{min} mice were cultured alone or co-cultured with WT IELs with or without a separation insert (Figure 14*A*). Although the number of live epithelial cells derived from the organoids co-cultured with WT IELs in the same well was reduced compared with organoids cultured alone, this reduction was canceled when co-cultured in the separated well (Figure 14*B* and *C*). These results suggest that the antitumor immune response of IELs is cell-to-cell contact-dependent.

We also checked the importance of CD103/E-cadherin signal in this system. APC^{min} organoids were co-cultured with WT IELs or Itgae$^{-/-}$ IELs (Figure 14*D*). As expected, the reduction of live epithelial cells derived from APC^{min} organoids co-cultured with WT IELs was canceled in the APC^{min} organoids co-cultured with Itgae$^{-/-}$ IELs group (Figure 14*E* and *F*). In addition, the number of recovered IELs from the Itgae$^{-/-}$ IELs group was smaller than that of the WT IELs group (Figure 14*G*). Both experiments suggest that the CD103/E-cadherin signal is essential for enough antitumor immune response in vitro, too.

Because the antitumor immune response of IELs was cell-to-cell contact-dependent and cytotoxic T cells expanded during it, we hypothesized that IELs suppress tumorigenesis by cytolysis. As shown in Figure 15, the percentage of 7-AAD$^+$ dead cells in the epithelial cells recovered from APC^{min} organoids co-cultured with WT IELs was higher than that from APC^{min} organoids alone, and this difference was reduced by the deletion of CD103, which supports our hypothesis.

Discussion

In previous studies, static analyses, such as histologic analysis, IHC, gene expression analysis, or flow cytometry, were performed to investigate the tumor microenvironment. In the current study, we succeeded in visualizing the 3D distribution of T cells in the tumor microenvironment by tissue clearing of whole-mount tissues and examining the T-cell dynamics and interactions between IELs and epithelial cells by an in vivo live-imaging system.

Although several reports have performed in vivo live-imaging of tumors, most involved a xenograft model injected with labeled immune cells.[26,27] In the current study, we developed T-cell–reporter mice with spontaneous intestinal tumors, which is more physiological than such models. With these models, we discovered that the movement of T cells in the microenvironment of intestinal tumors was restricted around the blood vessels and the interaction between IELs and epithelial cells was reduced.

The microenvironment of tumors is still enigmatic, and our tools will be very useful to visualize the 3D distribution and the dynamics of immune cells in the tumor microenvironment. The effect of immune checkpoint inhibitors on the T-cell dynamics in the tumor microenvironment may be worth exploring in future studies. Furthermore, analysis of dynamics in the tumor microenvironment may lead to novel strategies for cancer immunotherapy.

We also succeeded in creating a model to study the antitumor immune response of IELs in vitro by developing a

Figure 2. (***See previous page***). **Visualization of T-cell dynamics in the intestinal tumor microenvironment by an in vivo live-imaging system with the 2-photon microscope.** (*A*) Experimental design. Wide area images of live small intestinal tissues of (*B*) DPE–GFP × APC^{min} or (*C*) DPE–GFP mice. Green, GFP; blue, Hoechst 33342; red, intravenous dextran-tetramethylrhodamine; yellow, intraluminal dextran–Alexa Fluor 647. Histologic findings of small intestinal tissues of (*D*) DPE–GFP × APC^{min} or (*E*) DPE–GFP mice after in vivo live imaging. Z-stack images of live small intestinal tissues of (*F*) DPE–GFP × APC^{min} or (*G*) DPE–GFP mice. Time-lapse images of IELs of nontumor (N-T) region in (*H*) DPE–GFP × APC^{min} or (*I*) DPE–GFP mice. (*J*) Speed, (*K*) track length, (*L*) confinement ratio, and (*M*) total time of GFP$^+$ cells in contact with IECs were calculated (n = 3, each). Graphs show means ± SEM. Data were pooled from 3 independent experiments. SI, small intestinal.

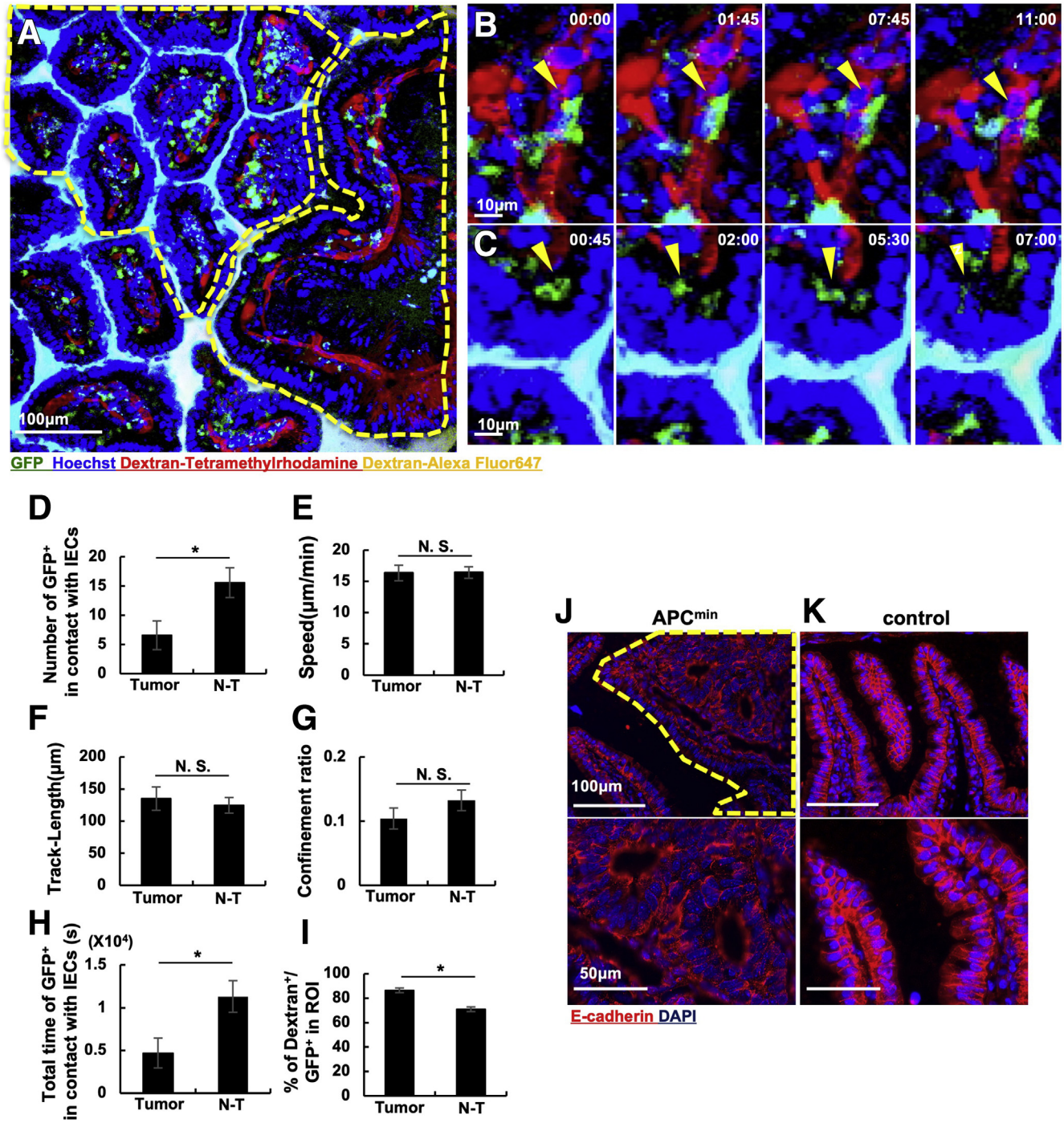

Figure 3. Cell-to-cell contact between small intestinal-IELs and epithelial cells is decreased in the intestinal tumor microenvironment. (*A*) Representative image of live small intestinal tissue with both tumor region and nontumor region in DPE–GFP × APC^{min} mice. Time-lapse images of (*B*) tumor region and (*C*) nontumor (N-T) region of DPE–GFP × APC^{min} mice. Green, GFP; blue, Hoechst 33342; red, intravenous dextran-tetramethylrhodamine; yellow, intraluminal dextran-Alexa Fluor 647. (*D*) Number, (*E*) speed, (*F*) track length, (*G*) confinement ratio, and (*H*) total time of GFP^{+} cells in contact with IECs (n = 8, each). (*I*) Percentage of GFP^{+} cells in contact with blood vessels (n = 10). Graphs show means ± SEM. Data were pooled from 8 independent experiments for panels *D–H* and are representative of similar independent 3 experiments for panel *I*. Histologic immunohistochemistry findings of small intestinal tissue of (*J*) DPE–GFP × APC^{min} or (*K*) DPE–GFP mice. Red, E-cadherin; blue, 4',6-diamidino-2-phenylindole (DAPI). *$P < .05$.

novel co-culture system of IELs and tumor organoids. We observed the destruction of the intestinal tumor structure and expansion of IELs and could capture the moment that IELs attack intestinal tumor cells. This system includes only IELs and tumor epithelium, without influence of other cells, such as myeloid cells, regulatory T cells, or mesenchymal

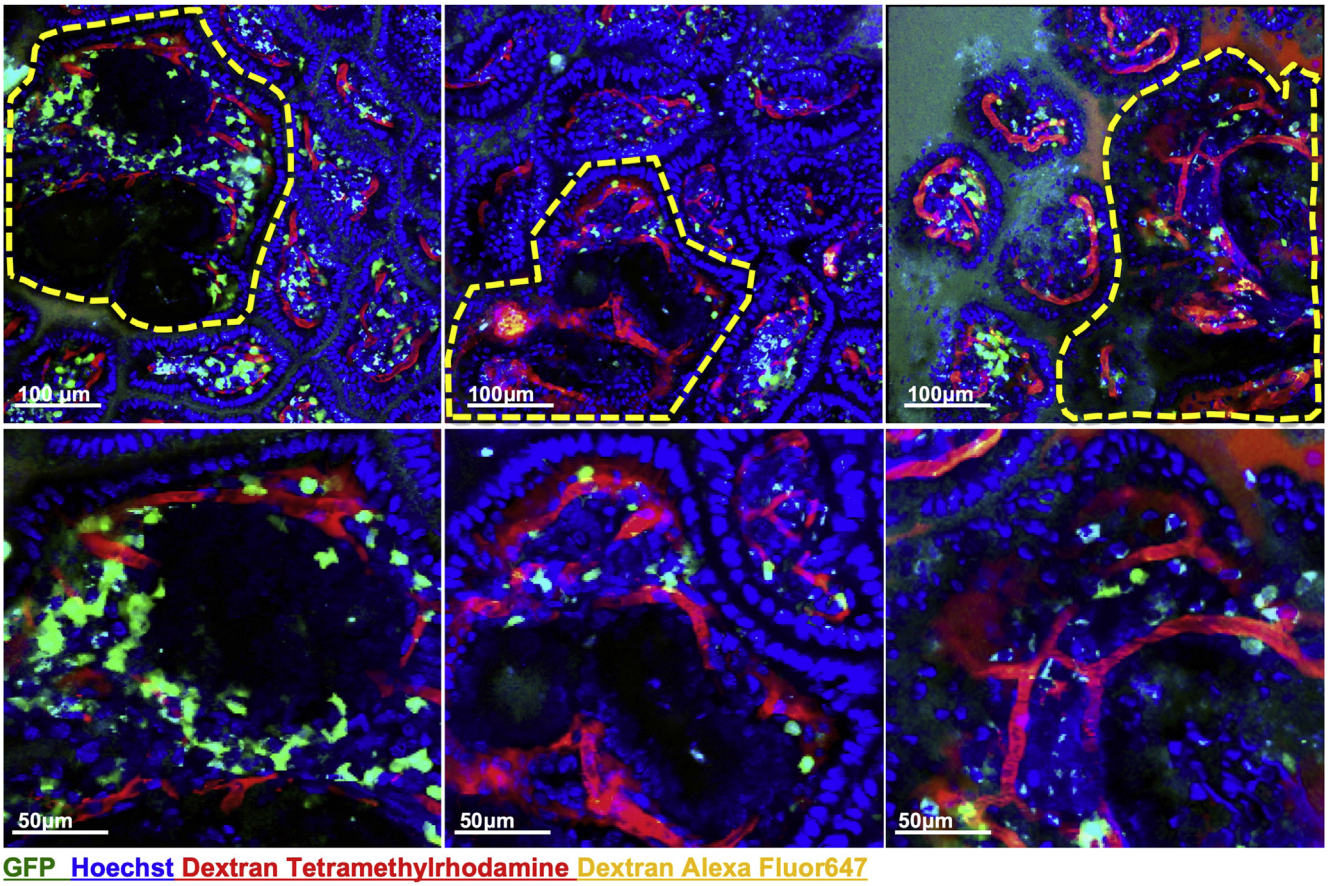

Figure 4. Visualization of the T-cell dynamics in small intestinal tumors. Still images of the 3 representative cases of in vivo live-imaging of the small intestinal tumors and T cells in the DEP–GFP × APC^{min} mice.

cells. In this system, antigen-presenting cells are not present, but IELs can recognize antigens of tumor epithelial cells by major histocompatibility complex-I or major histocompatibility complex-independent TCRs. For drug screening or comparison between subsets, an in vitro system is more useful than an in vivo system. In the future, we plan to identify the most important subsets for antitumor immunity and factors that enhance antitumor activity of IELs with this system.

Although previous studies showed that T cells play important roles in antitumor immunity, systemic T-cell deletion models mostly have been used. For example, 1 study showed that the number of intestinal tumors in APC^{min} × RAG$^{-/-}$ mice was higher than that in control mice. In contrast, the number of intestinal tumors in TCR$\beta^{-/-}$ or TCR$\delta^{-/-}$ mice was less than that of control mice, which was the result of the paradoxic increase of the other fraction of T cells.[17]

Although some studies have reported experimental mice in which the number of IELs was reduced, such as Itgae$^{-/-}$ or CC-chemokine receptor 9 (CCR9)$^{-/-}$ mice, complete deletion of IELs is difficult. In the current study, we proved that IELs and their cell-to-cell contact with IECs via CD103/E-cadherin signals play important roles for the anti-intestinal tumor immunity by combining in vivo live-imaging experiments, Itgae$^{-/-}$ × APC^{min} mice, and an in vitro co-culture system of IELs and intestinal tumor organoids. This report directly proves that IELs play important roles for anti-intestinal tumor immunity.

Determining whether humoral factors or cell-to-cell contact is important for antitumor immunity is difficult by T-cell deletion experiments only. In the current study, we showed that cell-to-cell contact with IECs was essential for the antitumor immune activity of IELs by combining Itgae$^{-/-}$ IEL–APC^{min} organoid co-culture and the Transwell system.

We also showed the importance of CD103/E-cadherin signals for the suppression of intestinal tumors. To the best of our knowledge, there are no drugs to increase the expression of CD103, however, several available drugs can increase the expression of E-cadherin. Celecoxib, a nonsteroidal anti-inflammatory drug, increased the expression of E-cadherin on IECs of APC^{min} mice,[28] although another study reported that celecoxib reduced the number of intestinal tumors in APC^{min} mice.[29] EMT inhibitors also affect E-cadherin expression. EMT involves the reduction of the epithelial markers including E-cadherin and an increase in mesenchymal markers on tumor cells, resulting in increased invasion and metastasis abilities.[22,23] Our results suggest that up-regulation of E-cadherin by these drugs may show important effects on anti-intestinal tumor activity.

Immune checkpoint inhibitors, an important focus in cancer immune therapy, enhance the antitumor activity of T

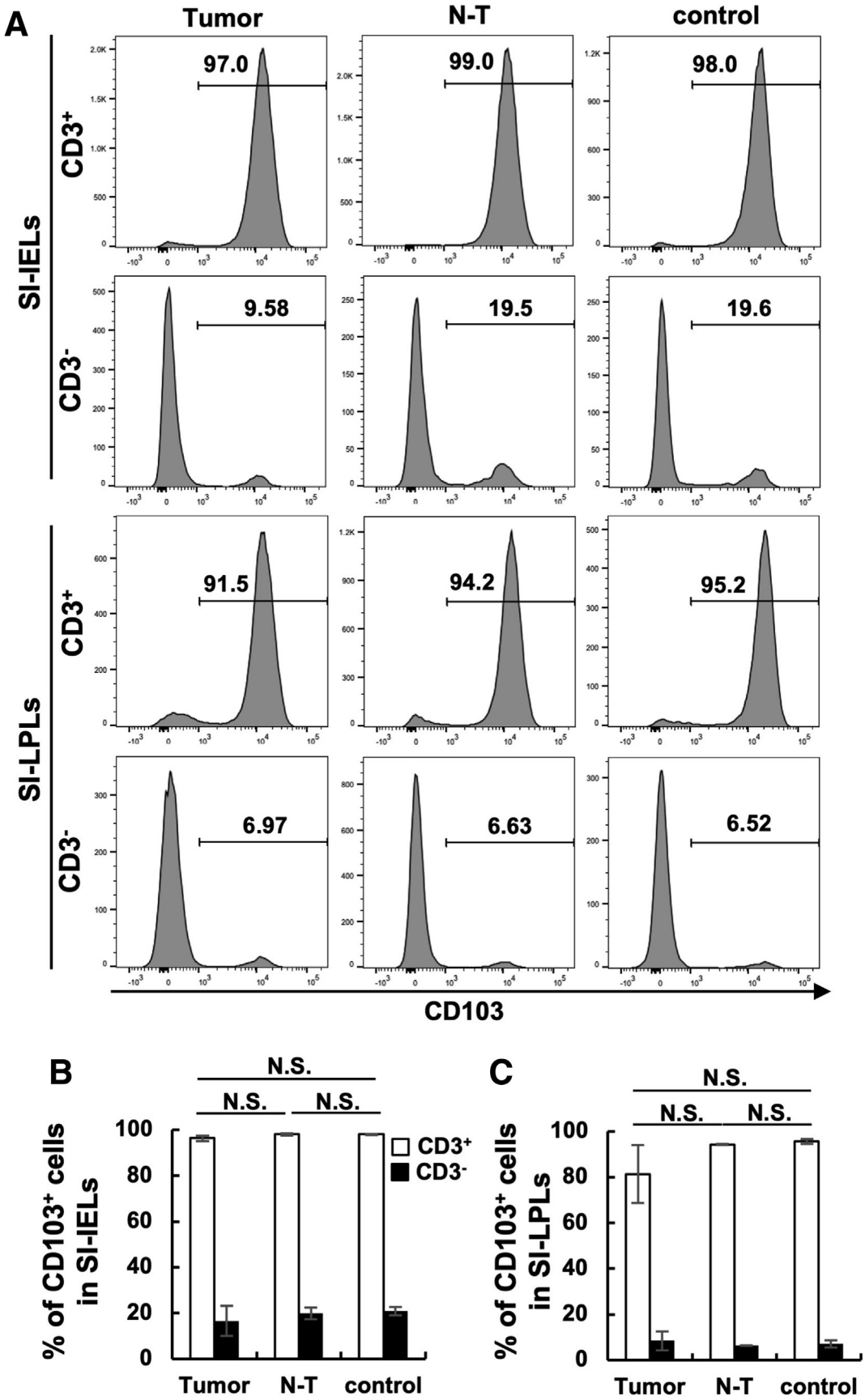

Figure 5. Expression of CD103 in T cells in the small intestine. (*A*) Representative histograms for CD103 gating in each group. Percentages of CD103$^+$ cells in CD3$^+$ and CD3$^-$ cells in (*B*) small intestinal (SI)-IELs or (*C*) SI-LPLs. Cells were recovered from tumor and nontumor (N-T) regions of APC^{min} mice and control WT mice (n = 3, each). Graphs show means ± SEM.

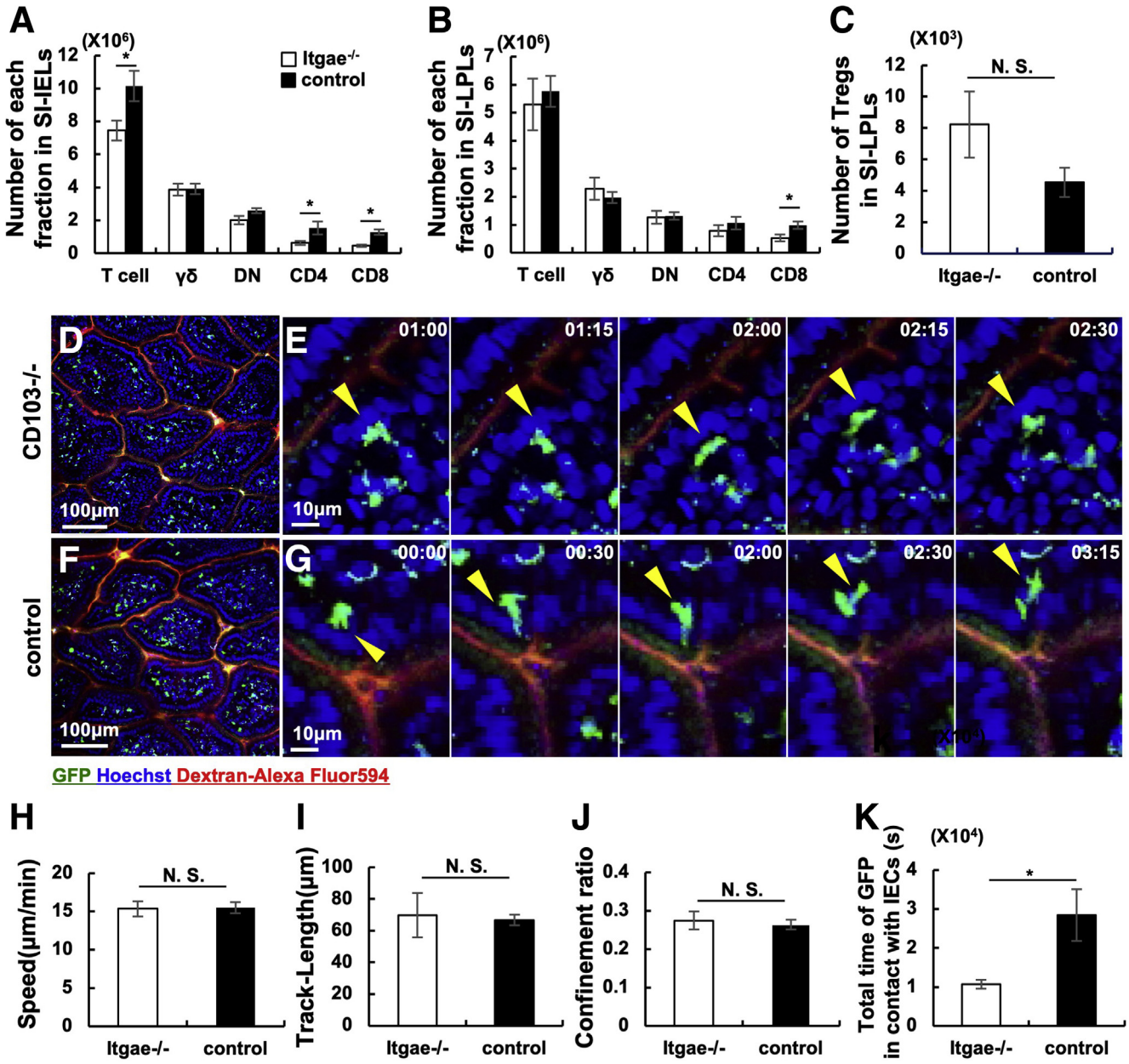

Figure 6. Cell-to-cell contact between small intestinal (SI)-IELs and epithelial cells is decreased in Itgae$^{-/-}$ mice. Number of T cells (CD3$^+$ cells), TCR $\gamma\delta$ (CD3$^+$TCR$\gamma\delta^+$TCRβ^- cells), DN (CD3$^+$TCRβ^+CD4$^-$CD8β^- cells), CD4$^+$ (CD3$^+$TCRβ^+CD4$^+$CD8β^- cells), and CD8$^+$ (CD3$^+$TCRβ^+CD4$^-$CD8β^+ cells) in (*A*) SI-IELs and (*B*) SI-LPLs, and (*C*) regulatory T cells (Tregs) (CD3$^+$CD4$^+$CD25$^+$Foxp3$^+$ cells) in SI-LPLs of Itgae$^{-/-}$ or littermate control mice (n = 8 in Itgae$^{-/-}$ mice and n = 9 in control mice). Graphs show means ± SEM. Data were pooled from 7 independent experiments. Representative images of live small intestinal tissues of (*D*) Itgae$^{-/-}$ × DPE–GFP or (*F*) control DPE–GFP mice. Time-lapse images of IELs of (*E*) Itgae$^{-/-}$ × DPE–GFP or (*G*) control DPE–GFP mice. Green, GFP; blue, Hoechst 33342; red, intraluminal dextran–Alexa Fluor 594. (*H*) Speed, (*I*) track length, (*J*) confinement ratio, and (*K*) total time of GFP$^+$ cells in contact with IECs (n = 6 each). Graphs show means ± SEM. Data were pooled from 6 independent experiments. *$P < .05$.

cells via cell-to-cell contact. Future studies should examine the combination of immune checkpoint inhibitors and strategies to increase cell-to-cell contact between IELs and epithelial cells.

Finally, our study may provide insight into the lower incidence rate of small intestinal cancers compared with colorectal cancers. We speculate that the abundance of IELs, which survey IECs and exclude tumor cells by cell-to-cell contact, may contribute to the low number of tumors in the small intestine. In contrast, this system may not work in the colon because of the sparseness of IELs.

In the future, drugs, foods, or gut microbes to increase the number of IELs in the colon or to enhance cell-to-cell contact between IELs and epithelial cells may be effective

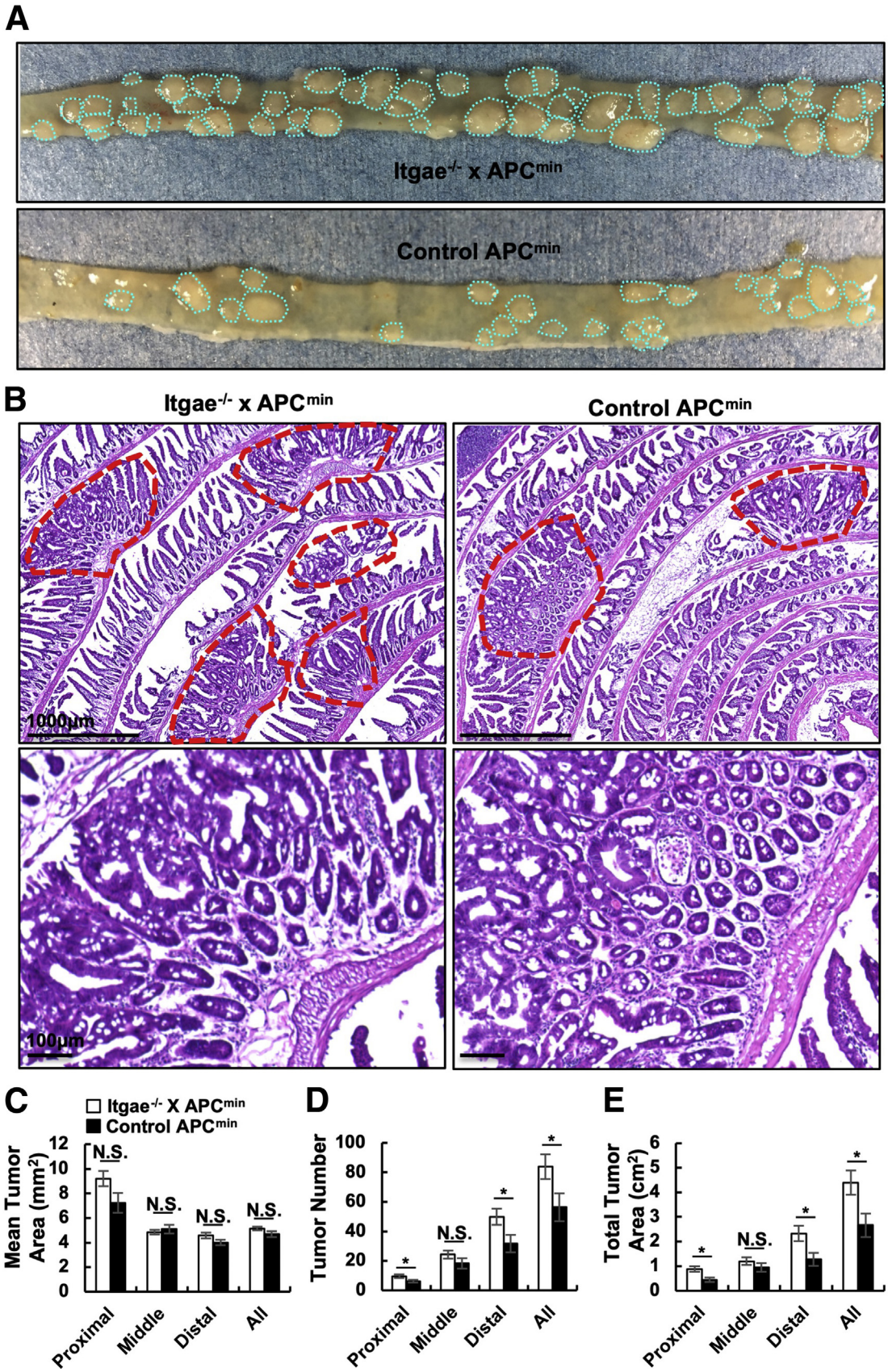

Figure 7. The number of intestinal tumors increased in Itgae$^{-/-}$ mice. (*A*) Representative images of gross appearance of ileum of Itgae$^{-/-}$ × APC^{min} and control APC^{min} mice. (*B*) Histologic findings of intestinal tumors of Itgae$^{-/-}$ × APC^{min} and control APC^{min} mice aged 16 weeks. (*C*) Mean area, (*D*) total number, and (*E*) total area of small intestinal tumors in female Itgae$^{-/-}$ × APC^{min} and control APC^{min} mice (n = 10 in Itgae$^{-/-}$ × APC^{min} mice and n = 8 in control APC^{min} mice). Graphs show means ± SEM. Data were pooled from 6 independent experiments. *$P < .05$.

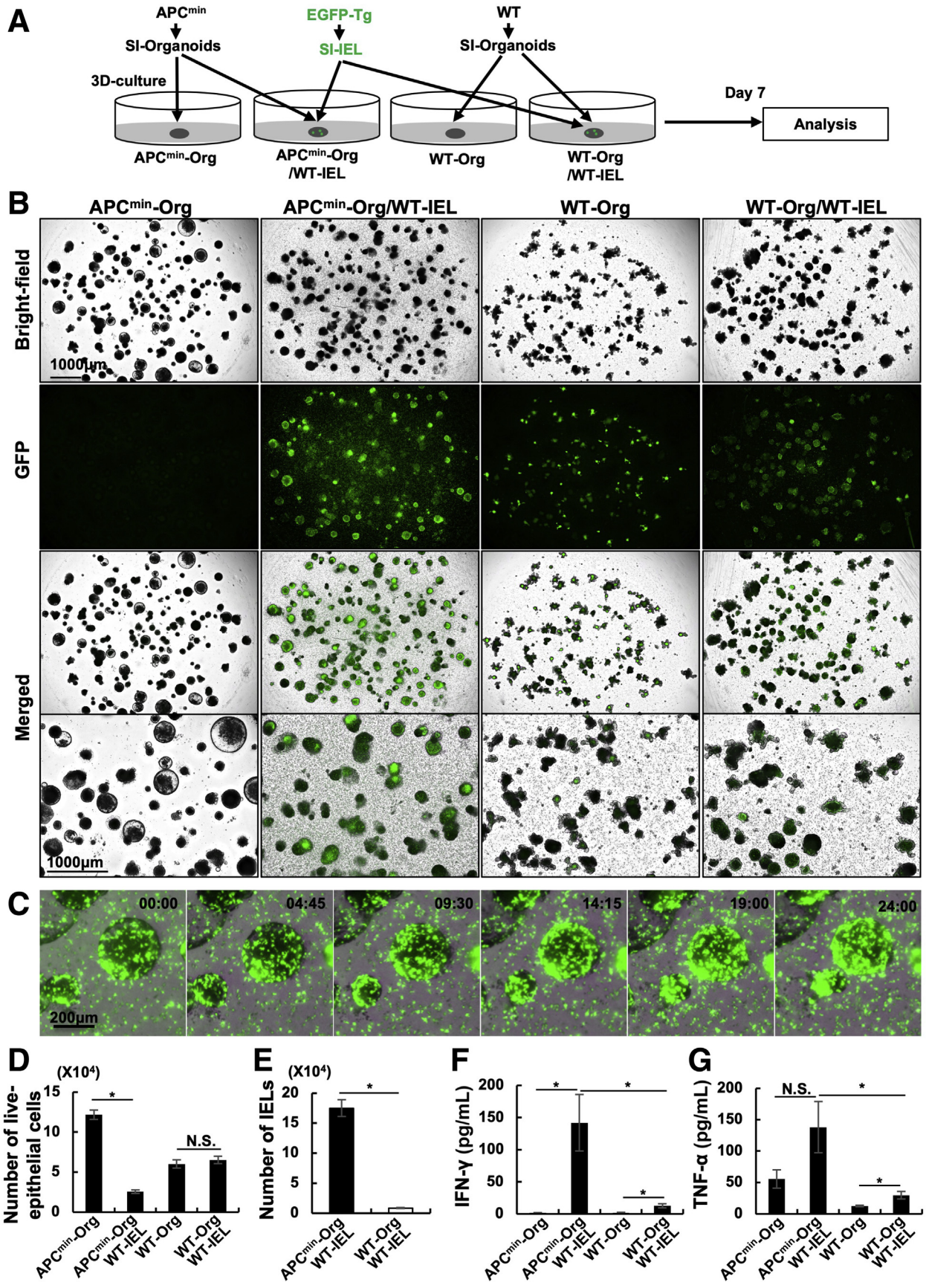
A
APCmin
SI-Organoids
EGFP-Tg
SI-IEL
WT
SI-Organoids
3D-culture
Day 7
Analysis
APCmin-Org
APCmin-Org /WT-IEL
WT-Org
WT-Org /WT-IEL
B
APCmin-Org
APCmin-Org/WT-IEL
WT-Org
WT-Org/WT-IEL
Bright-field
GFP
Merged
1000μm
C
00:00
04:45
09:30
14:15
19:00
24:00
200μm
D
(X10⁴)
Number of live-epithelial cells
N.S.
E
(X10⁴)
Number of IELs
F
IFN-γ (pg/mL)
G
TNF-α (pg/mL)
N.S.
APCmin-Org
APCmin-Org WT-IEL
WT-Org
WT-Org WT-IEL

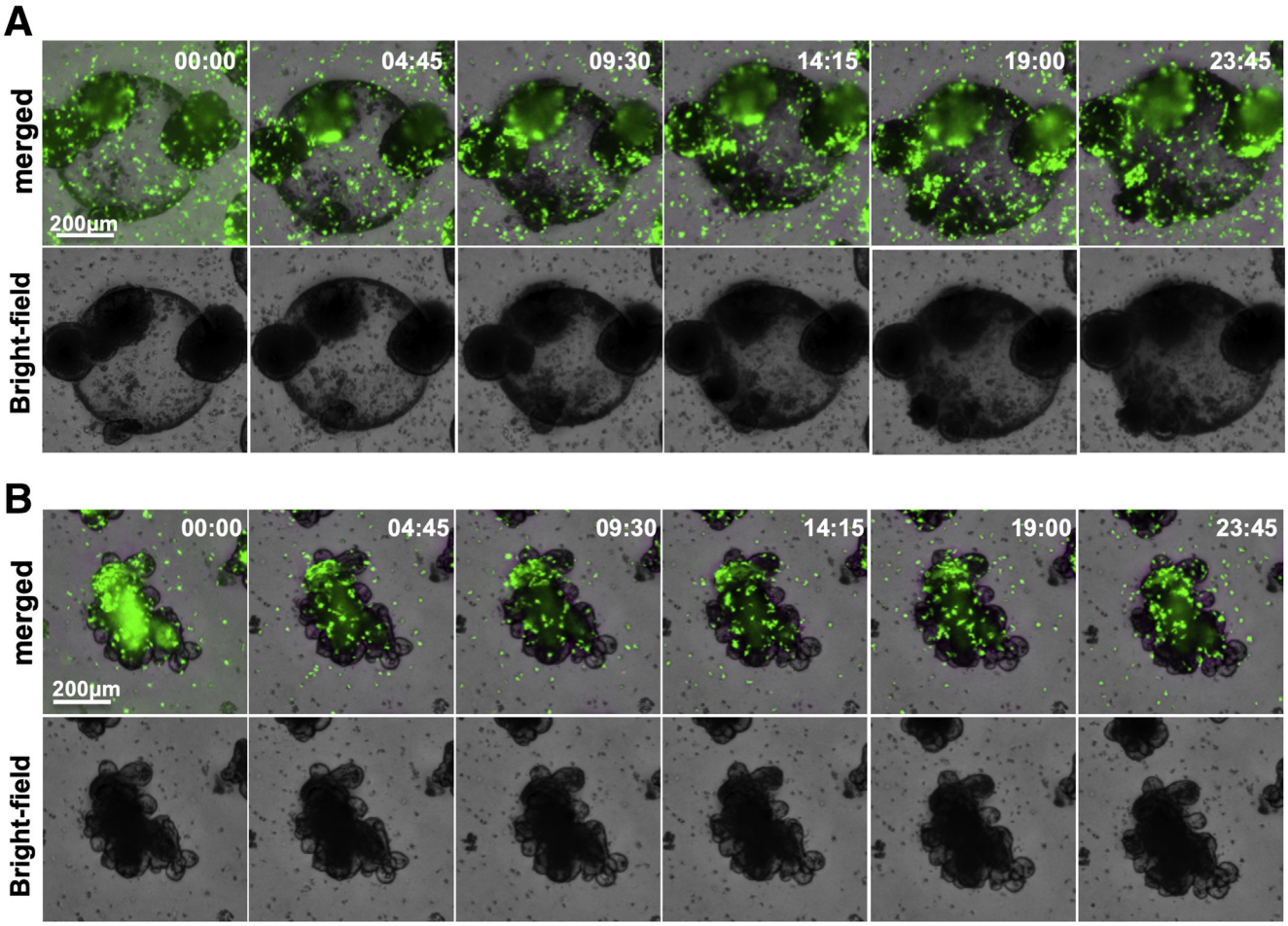

Figure 9. Time-lapse images of IELs and organoids. (*A* and *B*) Time-lapse images of in vitro co-culture of GFP IELs and (*A*) APC^{min} organoids or (*B*) WT organoids.

for the prevention of intestinal tumors in patients with a high cancer risk such as familial adenomatous polyposis.

Materials and Methods

Animals

C57BL/6 mice (age, 7–10 wk) were purchased from Japan CLEA (Tokyo, Japan). Itgae$^{-/-}$, APC^{min}, and EGFP mice were purchased from Jackson Laboratory (Bar Harbor, ME). DPE–GFP mice were kindly provided by the von Andrian Lab at Harvard Medical School (Boston, MA). Both male and female mice were used for experiments. We used Itgae$^{+/-}$ and Itgae$^{+/+}$ mice as a control for Itgae$^{-/-}$ mice. All mice were intercrossed and maintained under specific pathogen-free conditions at the Center for Experimental Animals at Tokyo Medical and Dental University. The Animal Study Committees approved all experiments, which were performed according to institutional guidelines and home office regulations.

Tissue Clearing

We rendered intestinal tissue transparent using Focus Clear (CelExplorer Labs Co, Hsinchu, Taiwan), according to the manufacturer's instructions. Briefly, anesthetized mice were injected intravenously with Hoechst 33342 (Thermo

Figure 8. (***See previous page***). **Antitumor immune response was provoked between co-cultured WT-IELs and intestinal tumor organoids.** (*A*) Experimental design. Organoids developed from the small intestine of WT or small intestinal tumor of APC^{min} mice were co-cultured with IELs from EGFP mice. After 7–9 days of co-culture, they were collected and dispersed into single cells. Numbers of cells were counted using flow cytometry. (*B*) Representative images of organoids and IELs after 7 days of co-culture. (*C*) Time-lapse images of APC^{min} organoids and IELs after 4 days of co-culture. (*D*) Number of live epithelial cells (7-AAD^{-}EpCAM^{+}CD45^{-} cells) collected from organoids in each group (n = 6–8). (*E*) Number of IELs (7-AAD^{-}GFP^{+} cells) in each group (n = 7–8). Graphs show means ± SEM. Data are representative of 2 similar independent experiments. (*F* and *G*) Evaluation of cytokines in the supernatant after 7 days of co-culture of organoids with IELs from WT mice. Concentration of (*F*) interferon (IFN)-γ and (*G*) tumor necrosis factor (TNF)-α (n = 6 each). Graphs show means ± SEM. Data were pooled from 2 independent experiments. *$P < .05$. Org, organoid; SI, small intestinal.

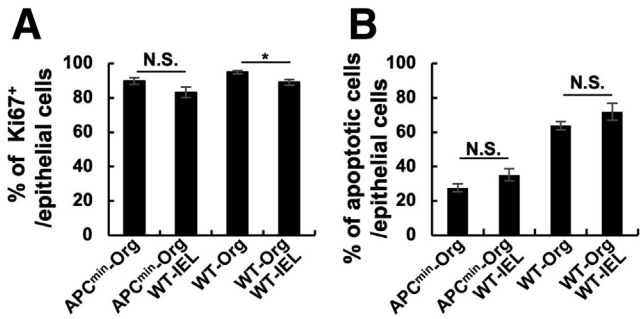

Figure 10. Evaluation of proliferation and early apoptosis of epithelial cells recovered from WT or APC^{min} organoids co-cultured with or without WT IELs. (*A*) Percentages of Ki67$^+$ cells in all epithelial cells (EpCAM$^+$ CD45$^-$ cells) recovered from cultured organoids in each group (n = 6–8). (*B*) Percentages of early apoptotic cells (AnnexinV$^+$7-AAD$^-$ cells) in all epithelial cells recovered from cultured organoids in each group (n = 6–7). Graphs show means ± SEM. Data were pooled from 2 independent experiments. *$P < .05$. Org, organoid.

Fisher Scientific, Waltham, MA) and dextran-tetramethylrhodamine (Thermo Fisher Scientific). After 30 minutes, mice were killed and the small intestinal tissue was collected, fixed, and incubated in Focus Clear. Samples were mounted on stage with Mount Clear (CelExplorer Labs Co). Z-stack images were taken at intervals of 0.425 μm using an A1RMP microscope (Nikon, Tokyo, Japan). Three planes were chosen at intervals of 131 slices, and GFP$^+$ cells were detected automatically according to the algorithm of Imaris software (Bitplane, Zurich, Switzerland). The number of cells in contact with blood vessels was counted manually.

In Vivo Live-Imaging

Anesthetized mice were injected intravenously with Hoechst 33342 (Thermo Fisher Scientific) and 70,000 molecular weight dextran-Texas Red (Thermo Fisher Scientific) or 2,000,000 molecular weight dextran-tetramethylrhodamine (Thermo Fisher Scientific) as necessary. A small incision was made on the abdomen and the small intestine was exposed. Mice were fixed on a customized stage for in vivo imaging and the temperature of core and exposed intestine was maintained at 37°C with a heating plate. The small intestine was gently opened along the antimesenteric border. Next, 10,000 molecular weight dextran–Alexa Fluor 594 (Thermo Fisher Scientific), dextran–Alexa Fluor 647 (Thermo Fisher Scientific), or phosphate-buffered saline (PBS) was added on the luminal side and a coverslip was placed. Cell behavior was recorded for 12–20 minutes at intervals of 15 seconds. In vivo imaging was performed using an A1RMP microscope (Nikon). Postacquisition image analyses were performed, and time-lapse videos were obtained using NIS-Elements (Nikon) or Imaris software (Bitplane).

First, all tracks of GFP$^+$ cells in contact with IECs in 50 time points at 15-second intervals were defined manually. The total time that GFP$^+$ cells were in contact with IECs was calculated as follows. The time of GFP$^+$ cells in contact with IECs was calculated according to the number of time points included in each track as 15-second intervals. The total time indicates the sum from 50 time points. The speed and track length were calculated automatically by Imaris software (Bitplane). The speed of GFP$^+$ in contact with IECs indicates the mean of the average speed of all tracks of GFP$^+$ cells in contact with IECs at 50 time points at intervals of 15 seconds. The track length of GFP$^+$ in contact with IECs indicates the mean of the total length of all tracks of GFP$^+$ cells in contact with IECs at 50 time points at intervals of 15 seconds. The number of GFP$^+$ cells in contact with IECs is the mean of the number of GFP$^+$ cells in contact with IECs defined manually at 10 time points at 75-second intervals. The percentage of Dextran$^+$/GFP$^+$ refers to the mean of the number of Dextran$^+$GFP$^+$ cells in the region of interest (counted manually)/the number of GFP$^+$ cells in the region of interest (counted automatically) at 10 time points at 75-second intervals.

The nontumor region was defined as the region without tumor with the same area as the tumor region. The confinement ratio was determined by track displacement length (the distance between the initial position and the last position of cells) over track length.

Histologic Analysis

After the perfusion fixation, small intestinal tissue was collected, embedded in optimal cutting temperature compound and frozen (fresh-frozen tissues). For IHC, cryostat sections (8 μm) of fresh-frozen tissues were incubated with primary antibody (mouse E-cadherin antibody, clone 114420; R&D Systems, Minneapolis, MN) at 4°C overnight, followed by incubation with secondary antibody (donkey anti-rat IgG [heavy cahin+light chain] Alexa Fluor 594; Thermo Fisher Scientific) at room temperature for 1 hour. Cells then were stained with 4',6-diamidino-2-phenylindole for nuclei staining. For H&E staining, cryostat sections (6–8 μm) of fresh-frozen tissues were stained with H&E. Images were taken with a BZ-X710 microscope (Keyence, Osaka, Japan).

Isolation of Mononuclear Cells From Murine Organs

Spleen was mashed and filtered through nylon mesh. Ammonium chloride potassium lysis buffer was used to lyse red blood cells from splenocytes. To isolate intestinal IELs and LPLs, we followed a modified protocol from a previous report.[30] First, Peyer's patches were removed from the small intestine. Next, half-lengths (for the cell count analysis) or full lengths (for the sorting experiments) of the distal ileum, proximal ileum, distal jejunum, proximal jejunum, and duodenum were opened longitudinally; samples were washed with Hanks' balanced salt solution (HBSS) medium and cut into small pieces. The dissected mucosae were rotated gently (60 rpm) using a rotator for 12 minutes at 37°C with 40 mL HBSS medium containing 2 mmol/L EDTA. The supernatant and remaining mucosae were separated with the nylon mesh. The supernatant was

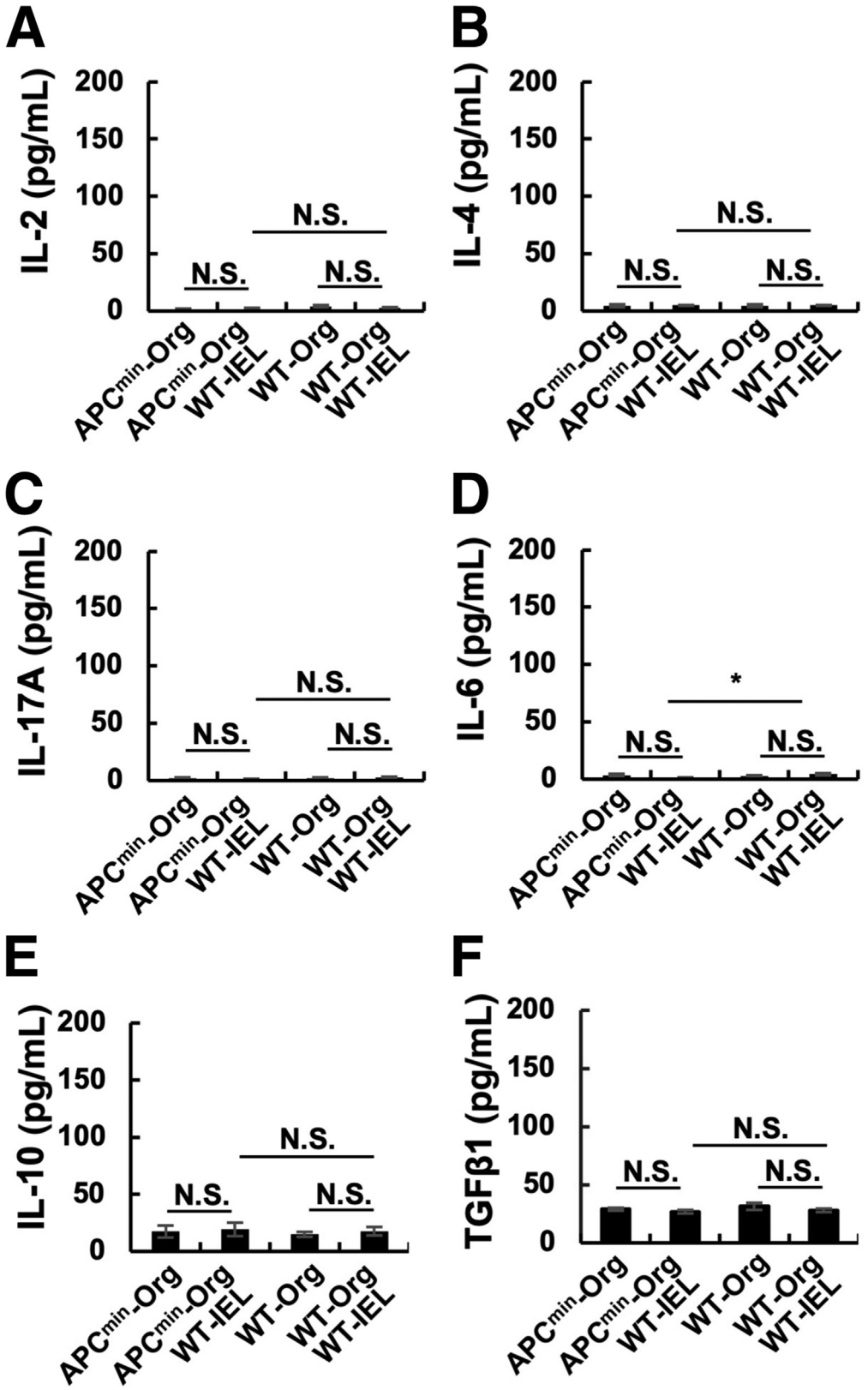

Figure 11. Evaluation of produced cytokines in the supernatant of in vitro culture of WT or APC^{min} organoids with or without WT IELs. Concentration of (*A*) IL2, (*B*) IL4, (*C*) IL17A, (*D*) IL6, (*E*) IL10, and (*F*) TGF-β1 in the supernatant of each group (n = 6 each). Graphs show means ± SEM. Data were pooled from 2 independent experiments. *$P < .05$. Org, organoid.

centrifuged and resuspended with 40% isotonic Percoll solution (GE Healthcare, Uppsala, Sweden) and then subjected to Ficoll–Hypaque density gradient centrifugation (40%/75%). IELs were collected as the layer between 40% and 75% Percoll. The remaining mucosae were rotated gently (60 rpm) using a rotator for 15 minutes at 37°C with 40 mL HBSS medium containing 0.5 mg/mL collagenase D (Roche) and 25 μg/mL DNase 1 (Roche, Mannheim,

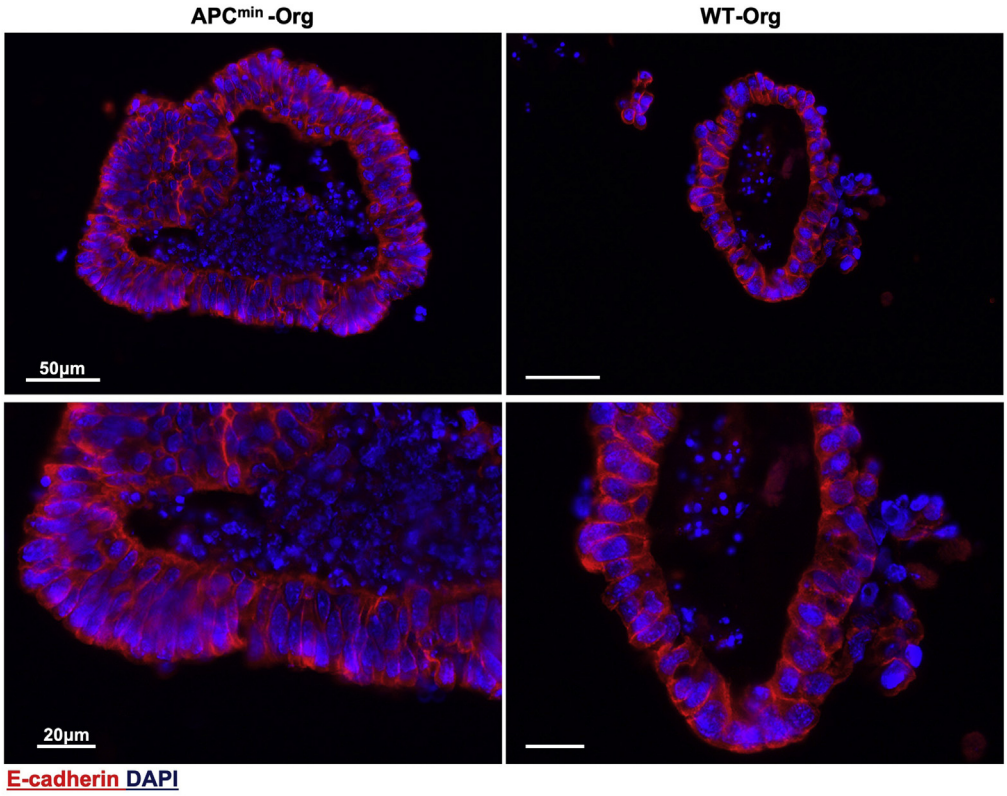

Figure 12. Immunohistochemistry of E-cadherin in the small intestinal organoids of APC^{min} or WT mice. Representative images of immunohistochemistry of fixed small intestinal organoids of APC^{min} or WT mice. Red, E-cadherin; blue, 4',6-diamidino-2-phenylindole (DAPI).

Germany. The mucosae then were filtered, centrifuged, and separated with Percoll. LPLs were collected as the layer between 40% and 75% Percoll. The number of T cells was counted manually using a hematocytometer.

Flow Cytometry Analysis and Reagents

To stain cell surface molecules, a single-cell suspension isolated from each organ was incubated with specific antibodies at 4°C for 20–30 minutes. For analysis, cells were resuspended with PBS and analyzed with FACSCanto II (BD Biosciences, Franklin Lakes, NJ). Data were analyzed with FlowJo software (BD Biosciences). The following antibodies were used for staining: anti-mouse CD3e-peridinin chlorphyll protein-cyanin (PerCP-Cy)5.5 (clone 145-2C11; BioLegend, San Diego, CA), anti-mouse CD3e–Alexa Fluor 488 (clone 145-2C11; BioLegend), anti-mouse TCRβ-allophycocyanin(APC)-Cy7 (clone H57-597; BioLegend), anti-mouse CD4-APC (clone RM4-5; BioLegend), anti-mouse

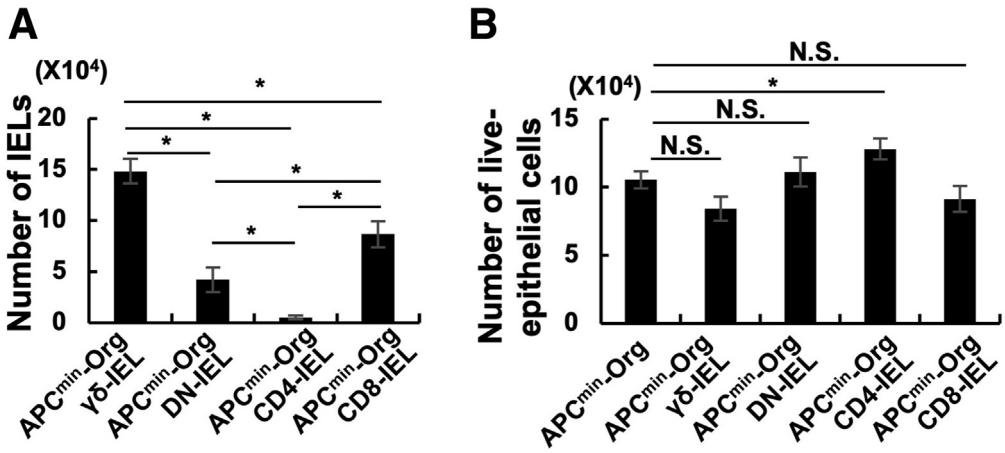

Figure 13. Co-culture of $\gamma\delta$, DN, CD4$^+$, or CD8$^+$ IELs from WT mice and APC^{min} organoids. (*A*) The number of recovered IELs (7-AAD$^-$EpCAM$^-$CD45$^+$ cells) in each group. (*B*) The number of live epithelial cells (7-AAD$^-$EpCAM$^+$CD45$^-$ cells) recovered from APC^{min} organoids in each group. Graphs show means ± SEM. Data were pooled from 2 independent experiments. n = 7–9 in each group. *$P < .05$. Org, organoid.

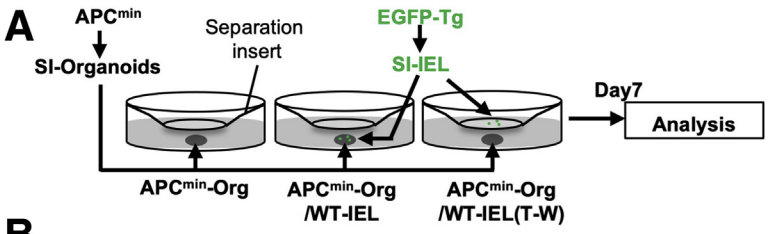
A
APCmin
SI-Organoids
Separation insert
EGFP-Tg
SI-IEL
Day7
Analysis
APCmin-Org
APCmin-Org /WT-IEL
APCmin-Org /WT-IEL(T-W)

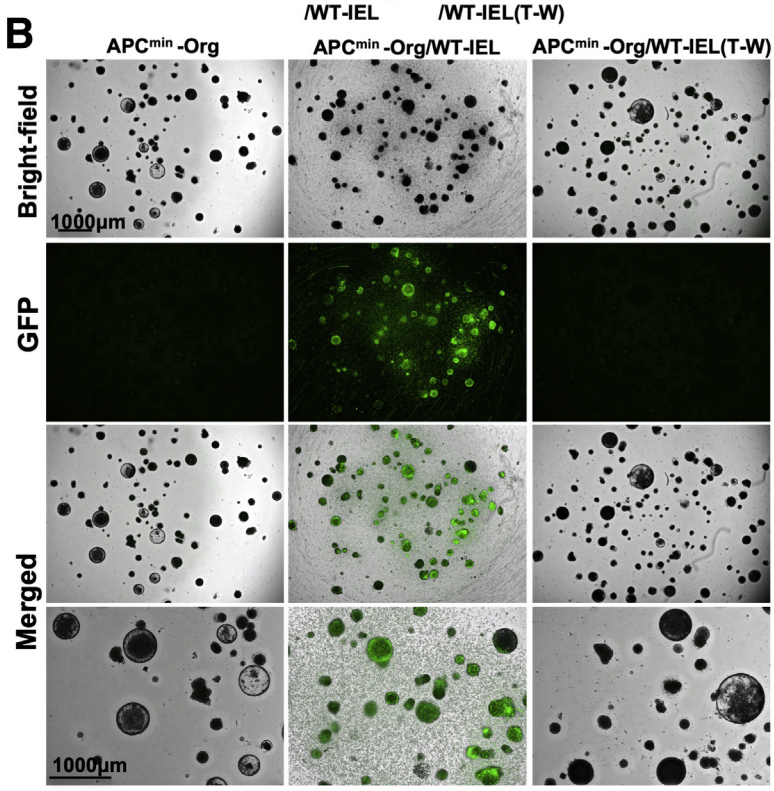
B
APCmin -Org
APCmin -Org/WT-IEL
APCmin -Org/WT-IEL(T-W)
Bright-field
GFP
Merged
1000μm

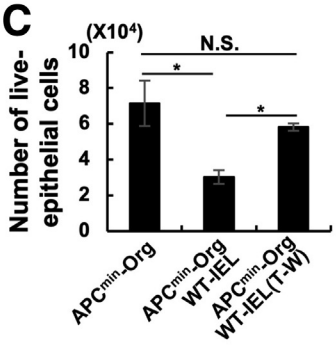
C
(X10⁴)
N.S.
*
*
Number of live-epithelial cells
0
2
4
6
8
10
APCmin-Org
APCmin-Org WT-IEL
APCmin-Org WT-IEL(T-W)

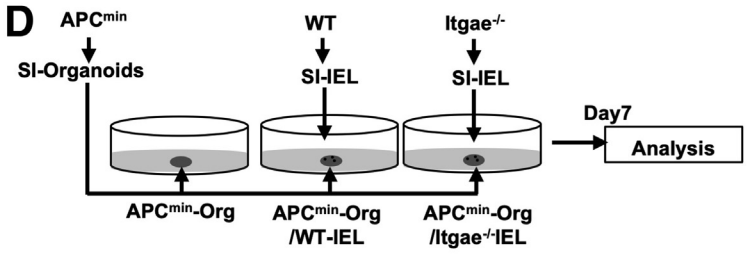
D
APCmin
SI-Organoids
WT
SI-IEL
Itgae-/-
SI-IEL
Day7
Analysis
APCmin-Org
APCmin-Org /WT-IEL
APCmin-Org /Itgae-/-IEL

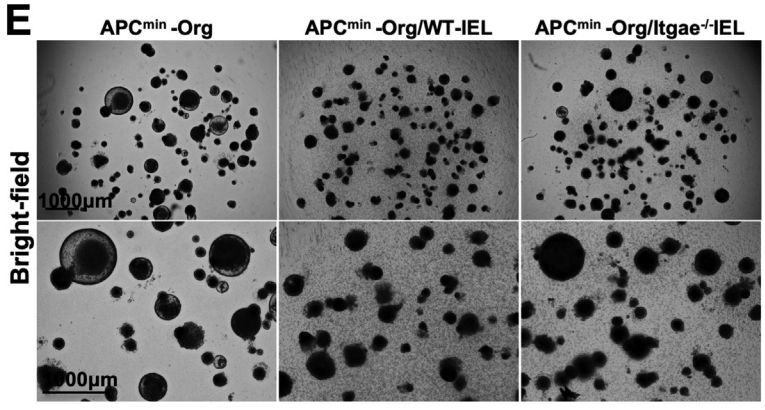
E
APCmin -Org
APCmin -Org/WT-IEL
APCmin -Org/Itgae-/-IEL
Bright-field
1000μm

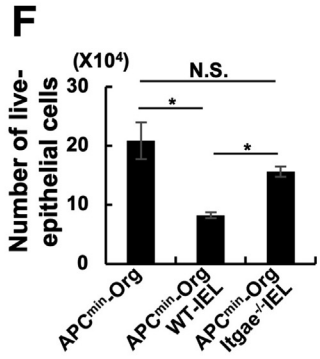
F
(X10⁴)
N.S.
*
*
Number of live-epithelial cells
0
10
20
30
APCmin-Org
APCmin-Org WT-IEL
APCmin-Org Itgae-/-IEL

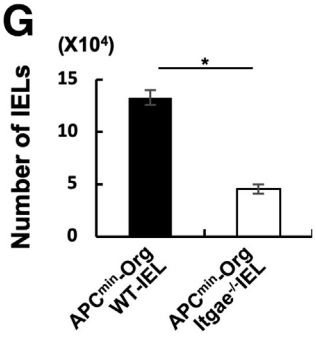
G
(X10⁴)
*
Number of IELs
0
5
10
15
APCmin-Org WT-IEL
APCmin-Org Itgae-/-IEL

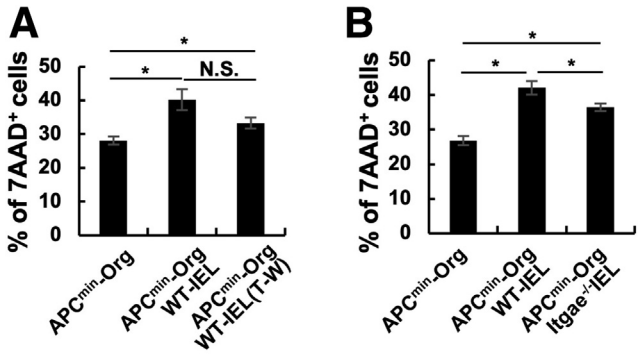

Figure 15. Evaluation of cell death of epithelial cells recovered from APC^{min} organoids co-cultured with or without IELs. (*A*) Percentages of 7-AAD$^+$ cells in epithelial cells (EpCAM$^+$CD45$^-$ cells) recovered from APC^{min} organoids in each group. Graphs show means ± SEM. Data were pooled from 2 independent experiments. n = 7–8 in each group. (*B*) Percentages of 7-AAD$^+$ cells in epithelial cells (EpCAM$^+$CD45$^-$ cells) recovered from APC^{min} organoids in each group. Graphs show means ± SEM. Data were pooled from 2 independent experiments. n = 9–11 in each group. *$P < .05$. Org, organoid; T-W, transwell.

CD8b-phycoerythrin (PE) (clone YTS156.7.7; BioLegend), anti-mouse CD8b-PerCP-Cy5.5 (clone YTS156.7.7; BioLegend), anti-mouse TCR$\gamma\delta$-PE-Cy7 (clone GL3; BioLegend), anti-mouse CD103-BV421 (clone 2E7; BioLegend), PE–anti-mouse CD103 (clone M290; BD Biosciences), anti-mouse CD8a–Alexa Fluor 488 (clone 5.3-6.7; BioLegend), anti-mouse CD4-PerCP-Cy5.5 (clone RM 4-5; BioLegend), anti-mouse CD3e–fluorescein isothiocyanate (FITC) (clone 145-2C11; Thermo Fisher Scientific), anti-mouse CD25-PE (clone PC61; BD Biosciences), anti-mouse forkhead boxprotein P3 (Foxp3)-APC (clone FJK-16a; Thermo Fisher Scientific), anti-mouse CD45-BV421 (clone 30-F11; BioLegend), anti-mouse epithelial cell adhesion molecule (EpCAM)-APC (clone G8.8; BioLegend), and anti-mouse Ki67–Alexa Fluor 488 (clone 16A8; BioLegend). The 7-AAD Viability Staining Solution (BioLegend) was used for dead cell removal, the Foxp3 staining kit (Thermo Fisher Scientific) was used for intracellular staining, and the FITC Annexin V Apoptosis Detection Kit with 7-AAD (BioLegend) was used for the evaluation of the type of death.

Quantification of Intestinal Tumors in APC^{min} Mice

Small intestines were collected from the killed mice aged 14–16 weeks and cut into 3 segments of the same length. Each segment was cut open longitudinally, washed with PBS, set on blue sheets, and images were taken. We analyzed the tumor area with ImageJ software (National Institutes of Health, Bethesda, MD).

Preparation of Small Intestinal Organoids

Crypts were isolated from the small intestine of male WT mice aged 7–11 weeks or small intestinal tumors of female APC^{min} mice aged 21 weeks as previously described.[24] One mouse was used for each isolation. The crypts were embedded in Matrigel (Corning, Corning, NY). Advanced Dulbecco's modified Eagle medium/F12 (Thermo Fisher Scientific) containing 50 ng/mL mouse Epidermal Growth Factor (mEGF) (Peprotech, Rocky Hill, NJ), 100 ng/mL mouse Noggin (mNoggin) (R&D Systems), 100 U/mL penicillin/streptomycin (Nacalai, Kyoto, Japan), 10 mmol/L HEPES (Nacalai), 2 mmol/L GlutaMAX-1 (Thermo Fisher Scientific), 1 mmol/L N-acetylcysteine (Sigma, St. Louis, MO), 1× N2 supplement (Thermo Fisher Scientific), 1× B27 supplement (Thermo Fisher Scientific), and 10 μmol/L Y-27632 (Wako, Osaka, Japan) were added to each well (complete medium). For WT organoids, 500 ng/mL mouse Rspondin1 (mRspondin1) (R&D Systems) was added. Organoids from APC^{min} mice were passaged at least once before co-culture with IECs.

Co-culture of IELs and Small Intestinal Tumor Organoids

We followed a modified protocol from a previous report.[25] Briefly, intestinal organoids were cultured for 2 days before co-culture with IELs. On the first day of co-culture, small intestinal (SI)-IELs collected from the WT mice aged 6–10 weeks were stained with anti-mouse TCRβ-APC-Cy7 (clone H57-597; BioLegend), anti-mouse CD4-APC (clone RM4-5; BioLegend), anti-mouse CD8b-PE (clone YTS156.7.7; BioLegend), anti-mouse TCR$\gamma\delta$-PE-Cy7 (clone GL3; BioLegend), and anti-mouse CD3e-FITC (clone 145-2C11; Thermo Fisher Scientific), and the $\gamma\delta$ (CD3$^+$TCR$\gamma\delta^+$TCRβ^-), DN (CD3$^+$TCRβ^+CD4$^-$CD8β^-), CD4$^+$ (CD3$^+$TCRβ^+CD4$^+$CD8β^-), and CD8$^+$ (CD3$^+$TCRβ^+CD4$^-$CD8β^+) IELs were sorted using FACSMelody (BD Biosciences) and MoFlo-XDP (Beckman Coulter, Brea, CA) in the co-culture with each of 4 subsets of IELs, and EGFP mice aged 7–30 weeks, WT mice aged 6–14 weeks, or Itgae$^{-/-}$ mice aged 8–14 weeks were stained with anti-mouse CD3e-PerCP-cy5.5 (clone 145-2C11; BioLegend) and the IELs (CD3$^+$ cells) were sorted using FACSMelody (BD Biosciences) in other experiments. Cultured organoids released from Matrigel were washed and counted. We

Figure 14. (*See previous page*). **Antitumor immune response of IELs against intestinal tumor organoids is cell-to-cell contact-dependent.** (*A*) Experimental design. Organoids developed from a small intestinal tumor of APC^{min} mice were co-cultured with IELs from EGFP mice with or without a separation insert. (*B*) Representative images of organoids and IELs after 7 days of co-culture. (*C*) Number of live epithelial cells (7-AAD$^-$EpCAM$^+$CD45$^-$ cells) collected from organoids in each group (n = 7–8). Graphs show means ± SEM. Data were pooled from 2 independent experiments. (*D*) Experimental design. Organoids developed from a small intestinal tumor of APC^{min} mice were co-cultured with IELs from WT or Itgae$^{-/-}$ mice. (*E*) Representative images of organoids and IELs after 7 days of co-culture. (*F*) Number of live epithelial cells (7-AAD$^-$EpCAM$^+$CD45$^-$ cells) collected from organoids in each group (n = 9–11). (*G*) Number of IELs (7-AAD$^-$EpCAM$^-$CD45$^+$ cells) in each group (n = 9–11). Graphs show means ± SEM. Data were pooled from 2 independent experiments. *$P < .05$. Org, organoid; SI, small intestinal; T-W, transwell.

combined 200 organoids and 2.0×10^5 IELs and centrifuged the samples for 3 minutes at $200 \times$ g. In the control group, the same number of organoids as the co-culture group was centrifuged. The pellet was suspended in 20 μL Matrigel and placed in 24-well plates. After Matrigel polymerization, 500 μL complete medium with 500 ng/mL mRspondin1, 100 U/mL recombinant human IL2 (Roche), 10 ng/mL mouse IL7 (Peprotech), and 10 ng/mL mouse IL15 (Peprotech) were supplemented. The medium was refreshed every 1–2 days. Images of organoids were taken with a BZ-X710 microscope (Keyence).

Co-culture of IELs and Small Intestinal Tumor Organoids With a Transwell System

A total of 200 organoids were embedded in 20 μL Matrigel in each well, with or without 2.0×10^5 IELs. A Millicell Cell Culture Insert (Merck, Darmstadt, Germany) filled with 20 μL Matrigel with or without 2.0×10^5 IELs was placed in each well. After Matrigel polymerization, 500 μL complete medium with mRspondin1 and cytokines in each well and 300 μL in insert were supplemented in a 24-well plate. The medium was refreshed every 2–3 days.

Cell Count of IELs and Organoids

Organoids and IELs were collected and centrifuged for 3 minutes at $400 \times$ g in the analysis for early apoptosis or $100 \times$ g in other experiments. The pellet was shaken (500 rpm) in the trypLE express (Thermo Fisher Scientific) containing 10 μmol/L Y-27632 (Wako) for 15 minutes at 37°C. After pipetting, cells were centrifuged for 3 minutes at $400 \times$ g, and the pellet was suspended with RPMI medium (Sigma). The numbers of live single epithelial cells and IELs were counted with FACSCanto II (BD Biosciences) and Count Bright Absolute counting Beads (Thermo Fisher Scientific).

In Vitro Live-Imaging of IELs and Intestinal Tumor Organoids

Time-lapse imaging of IELs and organoids in a 24-well plate was performed using a BZ-X710 microscope (Keyence) with a culture chamber, in which cells were cultured at 37°C, 5% CO_2. Pictures were acquired at intervals of 15 minutes over 24 hours.

Organoid Immunostaining

Organoids were cultured for 2 days in the same medium as used in the preparation of small intestinal organoids, released from Matrigel and embedded again. After 7 days of culture in the same medium as used in the co-culture with IELs, they were collected, fixed, embedded in OCT compound, and frozen. Immunostaining and evaluation were performed as described in the Histologic Analysis section.

Evaluation of Cytokines in Supernatant of Organoid Culture

Supernatant of organoid culture was collected. The evaluation of TGFβ1 was performed using the mouse/rat/porcine/canine TGF-β1 Quantikine Enzyme-Linked Immunosorbent Assay Kit (R&D Systems) and VERSA max (Molecular Devices, Tokyo, Japan) according to the manufacturer's instructions. Other cytokines were measured using the BD Cytometric Bead Array Mouse Th1/Th2/Th17 Cytokine Kit (BD Biosciences), FACSCanto II (BD Biosciences), and Flow Cytometric Analysis Program Array (BD Biosciences).

Statistical Analysis

Data are shown as means $\pm$ SEM. We examined the normality of the distribution of data in each group, using the Shapiro–Wilk normality test. For data without normality, statistical significance was determined with Mann–Whitney U tests. For data with normality, we used an unpaired Student t test for groups with equal variance or an unpaired Welch test for groups without equal variance. Statistical analysis was performed using Excel (Microsoft, Redmond, WA) or Prism software (GraphPad software, San Diego, CA).

References

1. Tang J, Yu JX, Hubbard-Lucey VM, Neftelinov ST, Hodge JP, Lin Y. The clinical trial landscape for PD1/PDl1 immune checkpoint inhibitors. Nat Rev Drug Discov 2018;17:854–855.
2. Darvin P, Toor SM, Sasidharan Nair V, Elkord E. Immune checkpoint inhibitors: recent progress and potential biomarkers. Exp Mol Med 2018;50:1–11.
3. Chen DS, Mellman I. Oncology meets immunology: the cancer-immunity cycle. Immunity 2013;39:1–10.
4. Whiteside TL. The tumor microenvironment and its role in promoting tumor growth. Oncogene 2008;27:5904–5912.
5. Arnold M, Sierra MS, Laversanne M, Soerjomataram I, Jemal A, Bray F. Global patterns and trends in colorectal cancer incidence and mortality. Gut 2017;66:683–691.
6. Araghi M, Soerjomataram I, Jenkins M, Brierley J, Morris E, Bray F, Arnold M. Global trends in colorectal cancer mortality: projections to the year 2035. Int J Cancer 2019;144:2992–3000.
7. Schottenfeld D, Beebe-Dimmer JL, Vigneau FD. The epidemiology and pathogenesis of neoplasia in the small intestine. Ann Epidemiol 2009;19:58–69.
8. Sekirov I, Russell SL, Caetano L, Antunes M, Finlay BB. Gut microbiota in health and disease. Physiol Rev 2010;90:859–904.
9. Elinav E, Nowarski R, Thaiss CA, Hu B, Jin C, Flavell RA. Inflammation-induced cancer: crosstalk between tumours, immune cells and microorganisms. Nat Rev Cancer 2013;13:759–771.
10. Moser AR, Luongo C, Gould KA, Shoemaker AR, Dove WF. ApcMin: a mouse model for intestinal and mammary tumorigenesis. Eur J Cancer 1995;31A:1061–1064.
11. Li Y, Kundu P, Seow SW, de Matos CT, Aronsson L, Chin KC, Kärre K, Pettersson S, Greicius G. Gut microbiota accelerate tumor growth via c-jun and STAT3 phosphorylation in APC Min/+ mice. Carcinogenesis 2012;33:1231–1238.

12. Cullen SP, Brunet M, Martin SJ. Granzymes in cancer and immunity. Cell Death Differ 2010;17:616–623.
13. van Acker A, Louagie E, Filtjens J, Taveirne S, van Ammel E, Kerre T, Elewaut D, Taghon T, Vandekerckhove B, Plum J, Leclercq G. The role of Ly49E receptor expression on murine intraepithelial lymphocytes in intestinal cancer development and progression. Cancer Immunol Immunother 2016; 65:1365–1375.
14. Cheroutre H, Lambolez F, Mucida D. The light and dark sides of intestinal intraepithelial lymphocytes. Nat Rev Immunol 2011;11:445–456.
15. Suzuki H. Age-dependent changes in intraepithelial lymphocytes (IELs) of the small intestine, cecum, and colon from young adult to aged mice. Arch Gerontol Geriatr 2012;55:261–270.
16. Rao VP, Poutahidis T, Ge Z, Nambiar PR, Boussahmain C, Wang YY, Horwitz BH, Fox JG, Erdman SE. Innate immune inflammatory response against enteric bacteria Helicobacter hepaticus induces mammary adenocarcinoma in mice. Cancer Res 2006;66:7395–7400.
17. Marsh L, Coleta PL, Hul MA, Selby PJ, Carding SR. Altered intestinal epithelium-associated lymphocyte repertoires and function in Apc Min/+ mice. Int J Oncol 2012;40:243–250.
18. Mrass P, Takano H, Lai GN, Daxini S, Lasaro MO, Iparraguirre A, Cavanagh LL, von Andrian UH, Ertl HCJ, Haydon PG, Weninger W. Random migration precedes stable target cell interactions of tumor-infiltrating T cells. J Exp Med 2006;203:2749–2761.
19. Agace WW. T-cell recruitment to the intestinal mucosa. Trends Immunol 2008;29:514–522.
20. Parker Sara Olson CM, Lefrancois L, Brenner MB, Jan Marsal MJ, Donohue JP, Her H, Beier DR, Adams CM, Strauch UG, Michael P, Schön WW, Arya A, Murphy EA. Mucosal T lymphocyte numbers are selectively reduced in integrin $^{\alpha}$E(CD103)-deficient mice. J Immunol 1999; 162:6641–6649.
21. Edelblum KL, Shen L, Weber CR, Marchiando AM, Clay BS, Wang Y, Prinz I, Malissen B, Sperling AI, Turner JR. Dynamic migration of $\gamma\delta$ intraepithelial lymphocytes requires occludin. Proc Natl Acad Sci U S A 2012;109:7097–7102.
22. Jung HY, Fattet L, Yang J. Molecular pathways: Linking tumor microenvironment to epithelial-mesenchymal transition in metastasis. Clin Cancer Res 2015;21:962–968.
23. Lee JM, Dedhar S, Kalluri R, Thompson EW. The epithelial-mesenchymal transition: new insights in signaling, development, and disease. J Cell Biol 2006; 172:973–981.
24. Sato T, Vries RG, Snippert HJ, van de Wetering M, Barker N, Stange DE, van Es JH, Abo A, Kujala P, Peters PJ, Clevers H. Single Lgr5 stem cells build crypt-villus structures in vitro without a mesenchymal niche. Nature 2009;459:262–265.
25. Nozaki K, Mochizuki W, Matsumoto Y, Matsumoto T, Fukuda M, Mizutani T, Watanabe M, Nakamura T. Co-culture with intestinal epithelial organoids allows efficient expansion and motility analysis of intraepithelial lymphocytes. J Gastroenterol 2016;51:206–213.
26. Boissonnas A, Fetler L, Zeelenberg IS, Hugues S, Amigorena S. In vivo imaging of cytotoxic T cell infiltration and elimination of a solid tumor. J Exp Med 2007; 204:345–356.
27. Lehmann S, Perera R, Grimm HP, Sam J, Colombetti S, Fauti T, Fahrni L, Schaller T, Freimoser-Grundschober A, Zielonka J, Stoma S, Rudin M, Klein C, Umana P, Gerdes C, Bacac M. In vivo fluorescence imaging of the activity of CEA TCB, a novel T-cell bispecific antibody, reveals highly specific tumor targeting and fast induction of T-cell-mediated tumor killing. Clin Cancer Res 2016; 22:4417–4427.
28. Carothers AM, Javid SH, Moran AE, Hunt DH, Redston M, Bertagnolli MM. Deficient E-cadherin adhesion in C57BL/6J-Min/+ mice is associated with increased tyrosine kinase activity and RhoA-dependent actomyosin contractility. Exp Cell Res 2006;312:387–400.
29. Swamy M, Patlolla JMR, Steele VE, Kopelovich L, Reddy BS, Rao C. Chemoprevention of familial adenomatous polyposis by low doses of atorvastatin and celecoxib given individually and in combination to APC Min mice. Cancer Res 2006;66:7370–7377.
30. Weigmann B, Tubbe I, Seidel D, Nicolaev A, Becker C, Neurath MF. Isolation and subsequent analysis of murine lamina propria mononuclear cells from colonic tissue. Nat Protoc 2007;2:2307–2311.

Received October 22, 2020. Accepted January 19, 2021.

Correspondence
Address correspondence to: Yasuhiro Nemoto, MD, PhD, Department of Gastroenterology and Hepatology, Tokyo Medical and Dental University, Tokyo Ika Shika Daigaku, 1-5-45 Yushima, Bunkyo-ku, Tokyo, 1138510 Japan. e-mail: ynemoto.gast@tmd.ac.jp; fax: (81) 3-5803-0268.

Acknowledgments
The authors thank all members of Ryuihci Okamoto's Laboratory at the Tokyo Medical and Dental University for discussion and advice. The authors thank Gabrielle White Wolf, PhD, from Edanz Group (https://en-author-services.edanzgroup.com/ac) for editing a draft of this manuscript.

CRediT Authorship Contributions

Ryo Morikawa, MD (Formal analysis: Lead; Investigation: Lead; Validation: Lead; Writing – original draft: Supporting)

Yasuhiro Nemoto, MD, PhD (Conceptualization: Lead; Data curation: Lead; Formal analysis: Supporting; Funding acquisition: Lead; Investigation: Supporting; Methodology: Lead; Supervision: Lead; Validation: Lead; Writing – original draft: Lead; Writing – review & editing: Lead)

Yuki Yonemoto, MD (Investigation: Supporting)

Shohei Tanka, MD, PhD (Investigation: Supporting)

Yuria Takei, MD, PhD (Investigation: Supporting)

Shigeru Oshima, MD, PhD (Funding acquisition: Supporting; Supervision: Supporting)

Takashi Nagaishi, MD, PhD (Supervision: Supporting)

Kiichiro Tsuchiya, MD, PhD (Funding acquisition: Supporting; Supervision: Supporting)

Kengo Nozaki, MD, PhD (Methodology: Supporting)

Tomohiro Mizutani, MD, PhD (Methodology: Supporting)

Tetsuya Nakamura, MD, PhD (Methodology: Supporting; Supervision: Supporting)

Mamoru Watanabe, MD, PhD (Funding acquisition: Supporting; Supervision: Lead)

Ryuichi Okamoto, MD, PhD (Funding acquisition: Lead; Supervision: Lead)

Conflicts of interest
The authors disclose no conflicts.

Funding
This work was supported by Japan Society for the Promotion of Science (JSPS) KAKENHI grants 17K09371, 16K09391, 19K08437, 19H03634, and 19H01050; Japan Agency for Medical Research and Development (AMED) grants 19bm0404055h0001, 19bm0304001h0007, and 19bk0104008h0002; and a Naoki Tsuchida Research Grant.